UCRL-359

~~J. W. Rose~~
W. Linder 50-226

Protons and Deuterons Knocked out of Nuclei by 90 Mev. Neutrons

By

Herbert Frank York, Jr.
A.B. (University of Rochester) 1942
M.S. (University of Rochester) 1943

DISSERTATION

Submitted in partial satisfaction of the requirements for the degree of

DOCTOR OF PHILOSOPHY

in

Physics

in the

GRADUATE DIVISION

of the

UNIVERSITY OF CALIFORNIA

Approved:

. . . . . .

. . . . . .

. . . . . .

Committee in Charge

Deposited in the University Library . . . . . .
Date Librarian

DISCLAIMER

TABLE OF CONTENTS

PROTONS AND DEUTERONS KNOCKED OUT OF NUCLEI BY 90 MEV NEUTRONS

Herbert York

I. INTRODUCTION

The inelastic processes which take place when nuclei are bombarded by nucleons with energies up to a few tens of Mev, or by alpha particles of energies up to 50 Mev, are well described by Bohr's [1] theory of the compound nucleus. The fundamental idea of this process is the following. In this energy range the nucleon-nucleon cross section is of such a magnitude that the mean free path of the nucleon in nuclear matter is very small compared to nuclear dimensions; hence the impinging particle begins to lose its energy immediately upon entering the nucleus. The nucleons which it strikes in turn go only a short distance before they interact with other nucleons, and so very soon the energy of the incoming particle is more or less evenly distributed among all of the nuclear particles, including the impinging one which is now captured because it no longer has enough energy to escape. The nucleus, thus excited, may return to the ground state, either by gamma or particle emission; both of these processes being slow compared to the characteristic nuclear time (the time it takes for a nucleon of a few Mev to travel a distance of the order of a nuclear radius). Particle emission is slow essentially because in only a few of the many possible modes of excitation is sufficient energy concentrated on one particle to enable it to escape the nucleus.

From the above, and from the fact that for excitations of more than about 10 Mev particle emission is more probable than gamma emission, a few qualitative statements concerning what will happen in the de-excitation of the compound nucleus can be made. First, the secondary particles will generally be neutrons, since a smaller concentration of energy is needed in this case than for charged particle emission. The reason for this is that a charged particle requires some additional energy to take it over the coulomb barrier. Second, the number of secondaries will be roughly equal to the energy of the impinging particle divided by the binding energy per particle. Third, there will be no correlation between the direction of the emitted and impinging particles, except for a slight concentration forward due to the comparatively low velocity acquired in the collision by the compound nucleus.

Since a basic assumption of this theory is that the mean free path for nucleons in nuclear matter is very small compared to nuclear dimensions, we should expect the theory to break down, at least in part, at very high energies because of the decrease in nucleon-nucleon cross section with energy. That this breakdown might be expected in the case of bombardment by 90 Mev neutrons is shown by various experiments done at the Radiation Laboratory. The total 90 Mev neutron cross section measurements of McMillan [2] et al, and the total and inelastic cross section measurements of DeJuren and Knable [3] and Rewtemahl et al[4] show a considerable "transparency" in the case of light nuclei in particular, which indicates

qualitatively that the mean free path for these neutrons in nuclear matter is of the order of the nuclear radius. From data of this type, Fernbach, Serber and Taylor [5] have calculated that the mean free path is 4.5×10^{-13}. A value close to this was also previously estimated by Goldberger[6]. The mean free path is the same in all nuclei because of the constant density of nuclear matter.

Qualitatively then, the sequence of events in an inelastic process at these high energies might be expected to be the following.* The impinging neutron strikes a nucleon in the nucleus imparting to it an approximately arbitrary fraction of its energy.** This struck nucleon is most likely to be a proton because the n-p cross section is several times larger than the n-n cross section [7]. There are at this point two fast nucleons moving in the nucleus, which, because of their high energy, may either collide with additional particles or escape from the nucleus without further interaction. Thus the immediate emission of one or more fast particles may occur, followed by the formation of a relatively long-lived compound nucleus of the type described by Bohr. The fast secondaries may be either charged or uncharged without prejudice because of the relative smallness of the coulomb barrier. Furthermore, if one of the secondaries is a proton, its direction of emission would be expected to be correlated with that of the impinging neutron in roughly the same way as in n-p scattering, that is faster ones forward, slower ones at larger angles relative to the neutron beam.

---

*Analyses similar to the following, pertaining primarily to high energy cosmic ray star fragments, have been given by W. Heisenberg in the Leipziger Berichte, 89, 369 (1937) and by E. Bagge in Ann. Phys., 37, 595 (1941).

**We automatically include the possibility of charge exchange by saying that the fraction transferred is arbitrary.

A detailed calculation of these predictions has been given in a paper by M. L. Goldberger [6], where he has taken into account such factors as the internal motion of the nucleons in the nucleus and the effect of the exclusion principle in a nuclear system considered as a degenerate Fermi Gas.

The object of the present work was an experimental investigation of these high energy charged secondaries. The nuclei investigated were carbon, copper and lead. The observed phenomena do not follow very closely Goldberger's detailed analysis, but do follow the above qualitative features, except for one important exception, namely a comparatively large yield of secondary deuterons and tritons.

Observations of this latter phenomenon were made simultaneously and reported by High Bradner[8] (using photographic plates) and K. Brueckner and W. Powell [9] (using a cloud chamber) as well as the author[10]. High energy deuterons have also been observed among the fragments from cosmic ray stars[11].

II. PRINCIPLES OF EXPERIMENTAL METHOD

A. Requirements

In this experiment we are concerned with measuring the angular and energy distributions of a mixture of several types of particles all of which have energies ranging from about twenty to one hundred Mev. The procedure used here is to measure the spectra at each of a series of angles, the angle under consideration being fixed by geometry.

For a known type of particle (i.e. proton, deuteron, or triton in the present case) the energy can be determined by a measurement of its $H\rho$, range, or specific ionization, and conversely, for a particle of known energy the type can be determined by any one of these three measurements. However, in the case of a mixture of particles, it is necessary to measure simultaneously any two of the above quantities in order to determine both the type and energy. Most of the measurements to be described here were made with the $H\rho$-specific ionization combination. The $H\rho$-range combination was used as a rough check on the results. As an extra check on some of the results, all three quantities were measured simultaneously in a few cases.

B. Relationships Between $H\rho$, Range, Specific Ionization, Charge, and Mass.

By using an empirical relationship between range and energy we can derive a number of useful connections between these various quantities. This relation is that the range of a charged particle (other than an electron) is proportional to its energy raised to the 1.8 power, the factor of proportionality being a function of the charge and mass of the particle.

and the nature of the material through which the particle is moving. This relation is quite accurate for protons between three Mev and several hundred Mev, and for other particles of corresponding velocity; although for the use we shall make of it, its degree of exactness is of no particular importance.

Hence, we have for a particle of mass m and charge q:

$$R = k(q, m) E^{1.8}$$

and therefore the specific ionization, I, is given by:

$$I = -\frac{dE}{dR} = \frac{1}{1.8\, k(q, m)\, E^{0.8}}$$

Now, it is well known that for non-relativistic energies I depends on E only through velocity, and that I is proportional to the square of the charge, so that

$$I \propto q^2 f\left(\frac{E}{m}\right)$$

and therefore

$$k(q, m) = \frac{k'}{q^2 m^{0.8}}$$

and so we have

$$R = \frac{k'}{q^2 m^{0.8}} E^{1.8}, \quad I = \frac{m^{0.8} q^2}{1.8 k' E^{0.8}}$$

where k' depends only on the material through which the particle is moving.

Combining these equations and the expression for energy in terms of Hρ: $\frac{p^2}{2m} = E = \frac{(He)^2}{2c^2} \frac{q^2}{m}$

we get the following useful relations:

$$I = k \frac{m^{1.6} \varepsilon^{0.4}}{(H\rho)^{1.6}}$$

$$H\rho = k' \frac{m^{0.72}}{\varepsilon^{0.44}} R^{0.28}$$

$$I = k'' \frac{\varepsilon^{1.11} m^{0.44}}{R^{0.44}}$$

where k, k', k'' depend only on the material through which the particle is moving.

By using these equations, we can calculate the following table:

TABLE I

Particle	For a fixed $H\rho$ the relative I is:	For a fixed range, the relative $H\rho$ is:	For a fixed range, the relative I is
Proton	1	1	1
Deuteron	3.03	1.65	1.36
Triton	5.80	2.21	1.63
He^3	7.65	1.63	3.52
Alpha	12.2	2.00	4.00

From the table one can see that the greatest difference in behavior for protons, deuterons and tritons occurs for a measurement of I for a fixed $H\rho$. The least distinction occurs in the case of the I-Range combination.

III. GENERAL EXPERIMENTAL METHOD

A. Arrangement of Components

Figure III-1 shows schematically the experimental arrangement used. The various components will be discussed in detail in Section IV.

90 Mev neutrons are produced by the stripping process [12] when 190 Mev deuterons strike the 1/2" Be target as shown in Figure III-1. These neutrons are collimated by a 2" hole through the concrete shielding surrounding the cyclotron and by the steel plug inserted into this hole as indicated in the Figure III-1. On emerging from this plug, the beam has a rectangular cross section of dimensions one inch by one and a half inches. The neutrons then pass between the poles of the particle analyzing magnet which is placed about six feet from the exit end of the collimator. The dimensions of the poles are 12" x 30", the pole gap is 1 3/4", and the field can be adjusted to any value up to 15,000 gauss. A scatterer is placed in the beam where it enters the magnet, and a slit defined by lead bricks is placed at the other end of the magnet. A counter telescope consisting of three proportional counters is placed as shown about 20" beyond the slit. Thus the charged secondaries from the scatterer travel along a circular path between the target and the slits, and along a straight path from the slits through the counters. From the radius of this orbit, and the value of the magnetic field, the $H\rho$ of the particle, and hence its energy, if its m and q are known, can be found. Figure III-2 shows a schematic diagram of the slit system and illustrates the determination of ρ and θ (the angle of emission of the particle relative to the direction of the neutron beam). It can be seen that

$$\rho = \frac{\overline{AB}}{2\sin\varphi} \qquad , \qquad \theta = \alpha - \varphi$$

where φ is the angle between the tangent line (axis of counter telescope) and the line connecting the scatterer and slit, and α is the angle between the direction of the neutron beam and this same line (AB). The uncertainty in ρ is very sensitive to the uncertainty in φ, the relation being as follows:

$$\frac{d\rho}{\rho} = -\cot\varphi \, d\varphi$$

and since

$$\frac{dE}{E} = 2\,\frac{d\rho}{\rho}$$

we have

$$\frac{dE}{E} = -2\cot\varphi \, d\varphi$$

Now, since the radii of curvature of the particles we are concerned with are large (60") compared to the dimensions of the magnet (30" x 12"), φ is quite small, being 15°. Therefore,

$$\frac{\Delta E}{E} \approx 8\,\Delta\varphi$$

where $\frac{\Delta E}{E}$ is the fractional error in E corresponding to an error of $\Delta\varphi$ in φ. Hence, an error of one degree in the determination of φ results in a 14% error in the value of E.

Because of this large potential error in the energy, it was deemed advisable to have an additional means of measuring the energy of the particles. Therefore, by means of a method to be described in Section IV-D, the particles themselves were made to measure the $H\rho$. The agreement between the measurements made by these two methods was quite good. For instance, at

0°, the radius as found from geometry was 60", and the radius as measured by the particles was 60.5".

B. Counter System for $H\rho$-Specific Ionization Method

In the $H\rho$-ionization method the first of the three counters in the telescope is used to determine the specific ionization of the particles, the other two, which are placed in electrical coincidence with the first, are used principally to eliminate the large number of unwanted pulses produced in the first tube by particles coming from random directions. The ionization produced in the first tube is measured by means of a ten channel pulse height analyzer constructed by Clyde Wiegand, and based on a Los Alamos model[13]. Absorbers can be placed in position A, allowing the making of a range measurement which can be used as an additional check on the nature of the radiation detected.

C. Counter System for $H\rho$-Range Method

In the $H\rho$-range measurement the same set up is used with the absorber at A now being an essential part of the apparatus. The range is determined by the method of desensitization of the last counter*. In this method, the lower limit of the range of a particle (and hence its energy if its charge and mass are determined by other means) is set by the thickness of the absorber A. An upper limit to its range is set by making the last counter sensitive only to those particles having more than some predetermined specific ionization, and hence having less than a certain residual range, since,

*This method was first tried and used successfully by Clyde Wiegand in connection with the n-p scattering experiments done at the Radiation Laboratory. See footnote 14 for references.

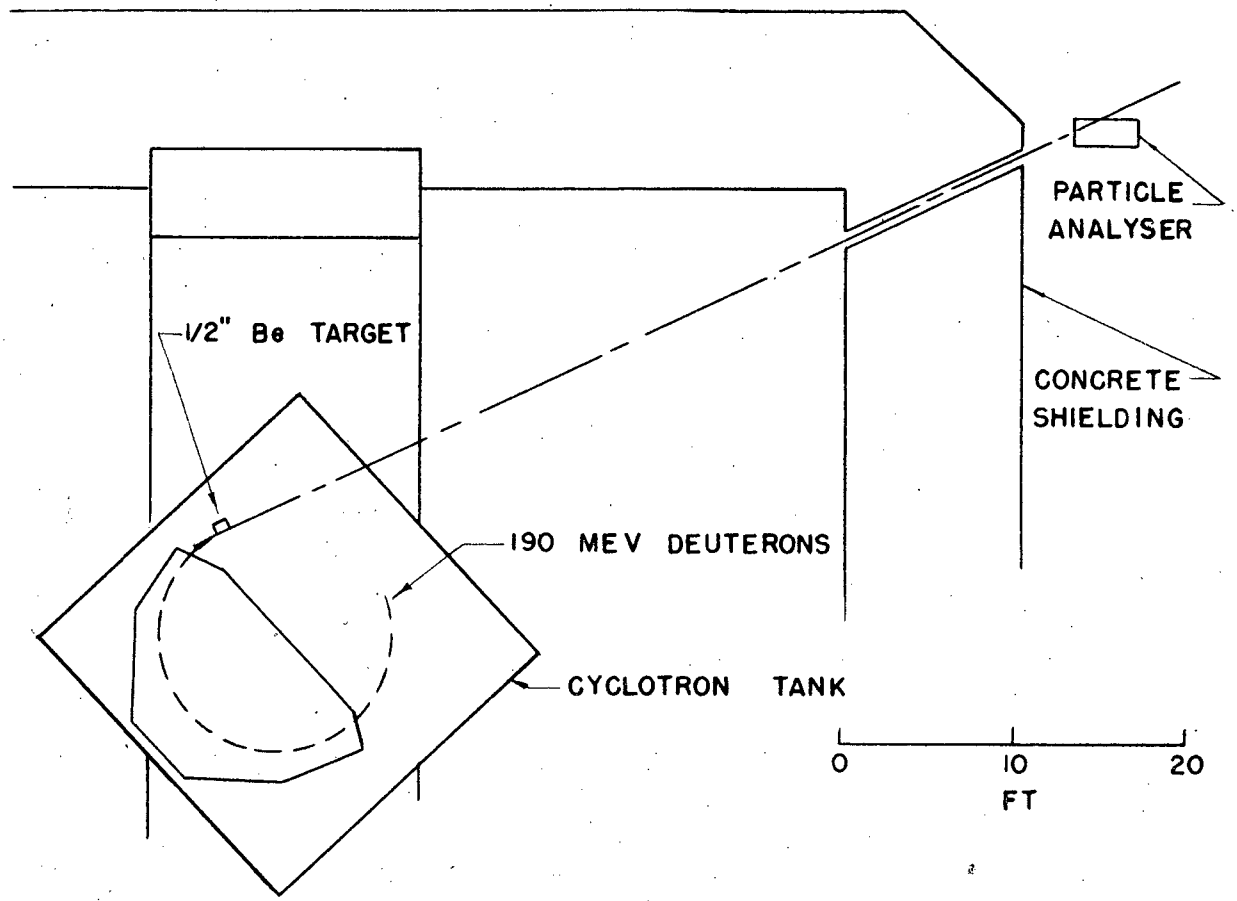
PARTICLE
ANALYSER
1/2" Be TARGET
CONCRETE
SHIELDING
190 MEV DEUTERONS
CYCLOTRON TANK
0
10
20
FT

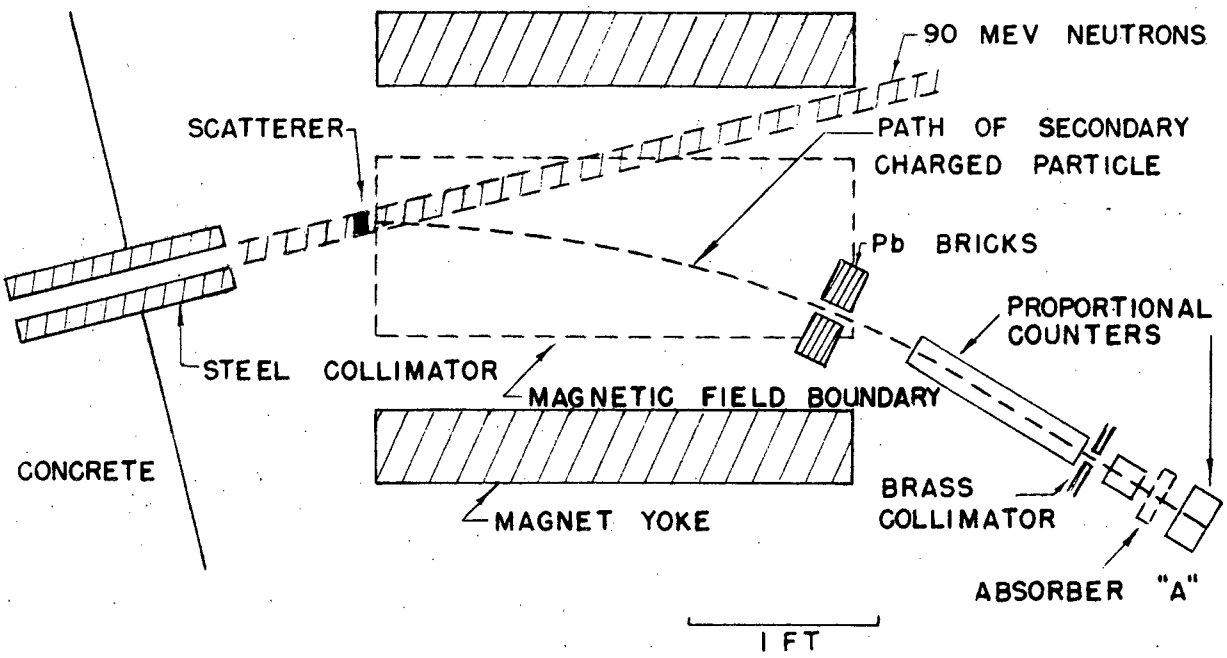
90 MEV NEUTRONS
SCATTERER
PATH OF SECONDARY
CHARGED PARTICLE
Pb BRICKS
PROPORTIONAL
COUNTERS
STEEL COLLIMATOR
MAGNETIC FIELD BOUNDARY
CONCRETE
MAGNET YOKE
BRASS
COLLIMATOR
ABSORBER "A"
1 FT

FIG. III -1

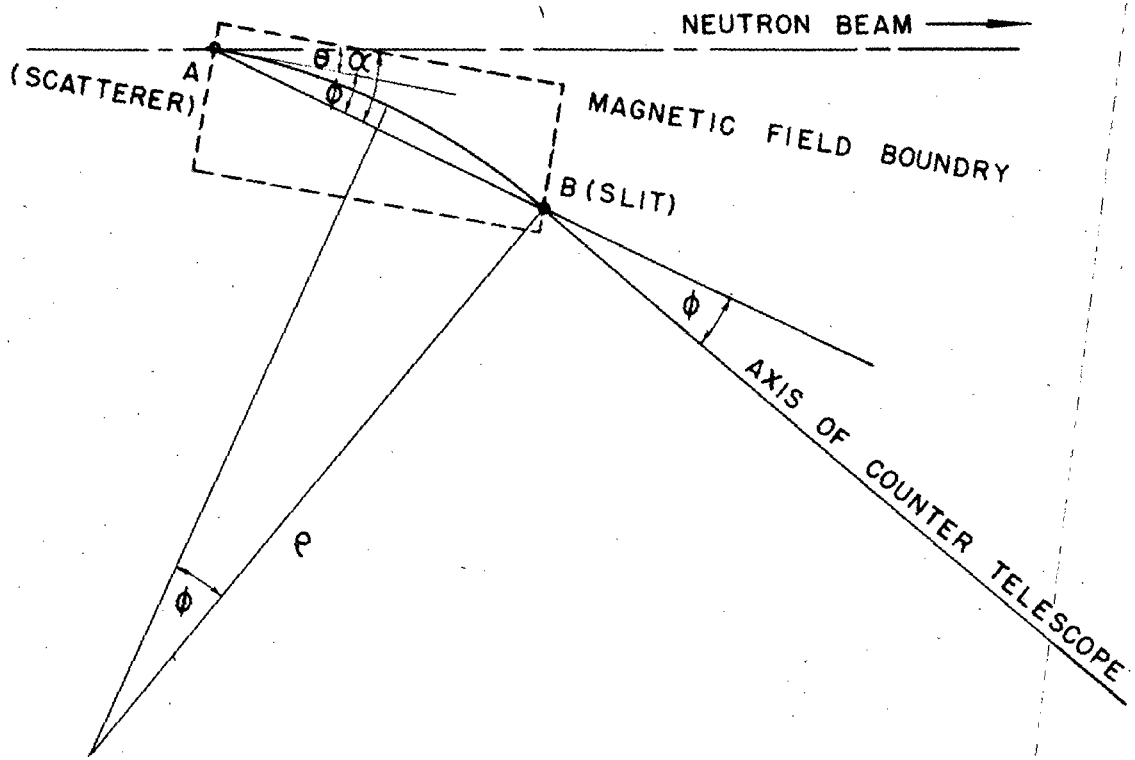

SCHEMATIC LAYOUT SHOWING DETERMINATION OF ρ & θ

FIG. III - 2

as shown in II, R is proportional to $I^{-9/4}$.

IV. DETAILS OF APPARATUS

A. The Neutron Beam

The neutron beam, produced and collimated as described in Section III, has a considerable energy spread. The spectrum as measured experimentally by Hadley et al[14] and Brueckner et al[15] in connection with n-p scattering experiments shows a peak with a maximum at about 90 Mev, and a half width of 25 to 30 Mev. Figure IV-1 is a reproduction of the spectrum as given in the paper by Hadley et al. The solid curve shown is the theoretical spectrum derived by Serber[12].

As described above, the beam is collimated to a rectangular cross section which measures 1" vertically and 1 1/2" horizontally. By placing a long copper bar in the neutron beam in such a way as to shield the scatterer from the direct beam of collimated neutrons, we have found that less than 1% of the effects reported in this paper are produced by neutrons other than those coming directly from the cyclotron.

B. Magnet

A photograph of the magnet is shown in Figure IV-2. It is one of three general utility magnets constructed at the Radiation Laboratory. The poles are rectangular and measure thirty by twelve inches; the pole gap is one and three quarters inches. The current to the coils is supplied by an electronically regulated motor generator set.

The field current calibration was made by Duane Sewell's magnetic measurements group. The field can be varied continuously from 1500 gauss up to 15,500 gauss. The coils are air cooled and consume 7500 watts

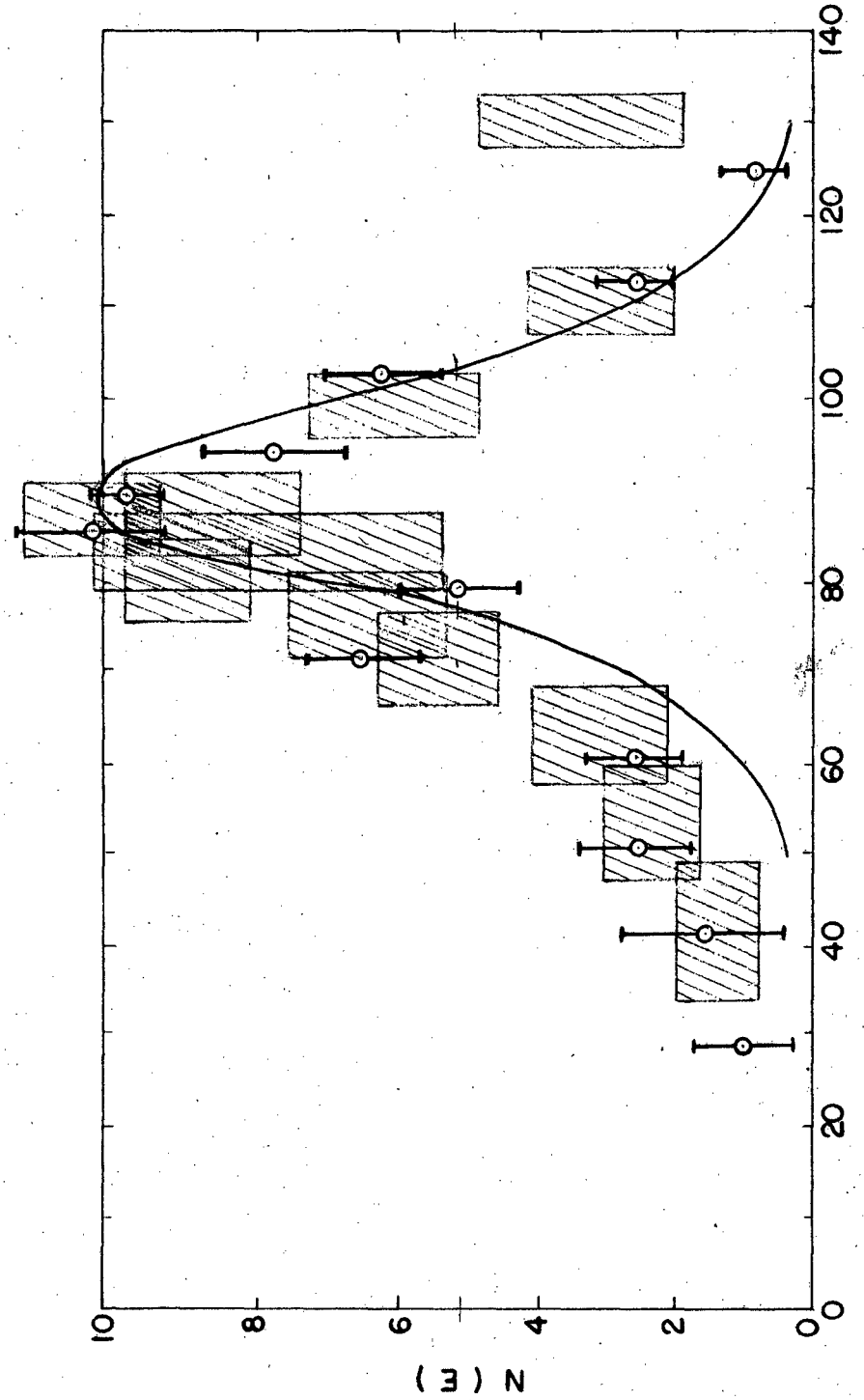

FIG IV - 1

(150 amperes, 50 volts) at the maximum field strength.

C. Scatterers and Slits

The scatterers are carbon, copper and lead rectangles three inches long and one-half inch wide. They are placed in the beam with the long dimension vertically, and with the three by one-half inch face normal to the direction of emission of the particular particles being studied. The scatterer thus subtends the entire beam vertically, but only a small portion of it horizontally.

The thickness of the scatterers in the direction of the emitted particles under study is determined by a compromise between getting enough secondary particles to work with and having a reasonably small energy loss in the scatterer. The value chosen was one-eighth inch for all three materials. Calculations showing the effects of the thickness on the measurements are given in Section VII.

The slit (placed as shown in Figures III-1 and III-2) was formed by placing two lead bricks in the magnet gap near one edge. The bricks were two inches thick and four inches long. The slit formed was one-half inch wide.

D. Proportional Counters

A detailed schematic drawing of the counter telescope is shown in Figure IV-2. The first tube is the one used to measure the specific ionization of the particles. In the energy range of interest here, the specific ionization is quite small, being for instance 6 kev/cm of Argon for 100 Mev protons. The first tube has therefore been constructed with a

useful length (essentially the length of the collecting wire) of 25 cm, so as to provide reasonably large pulses. Having the tube rather long compared to its diameter also aids in reducing the importance of end effects.

The construction of this counter is quite simple. It consists of a brass cylinder with an inside diameter of two inches, sealed at the ends with two mil dural windows which are held against rubber gaskets by a standard ring and flange arrangement. The anode of the counter is a five mil nickel wire supported at each end by heavier copper wires (.050") which pass through the walls of the tube through Kovar glass seals. The counter is evacuated and filled through a refrigerator valve placed as shown. The gas in the counter consists of 97% argon plus 3% CO_2 at about 1.1 atmospheres pressure. The counter is normally operated with the brass cylinder at ground potential, with the anode at about 1800 volts positive potential.

Various investigations of the operating characteristics of this counter were made by placing an alpha source (Po) inside in such a way as to emit alphas either along a line parallel to the anode or perpendicular to it. The gas amplification and the rate of change of gas amplification with collecting voltage (namely by a factor of two per hundred volts) were found to agree satisfactorily with results given by Diven and Rossi[16].

A typical spectrum of pulse heights from one of these Po sources is shown in Figure IV-4. The position of the source (in the filling tube) is also shown. The distribution is seen to consist of a peak with a half-

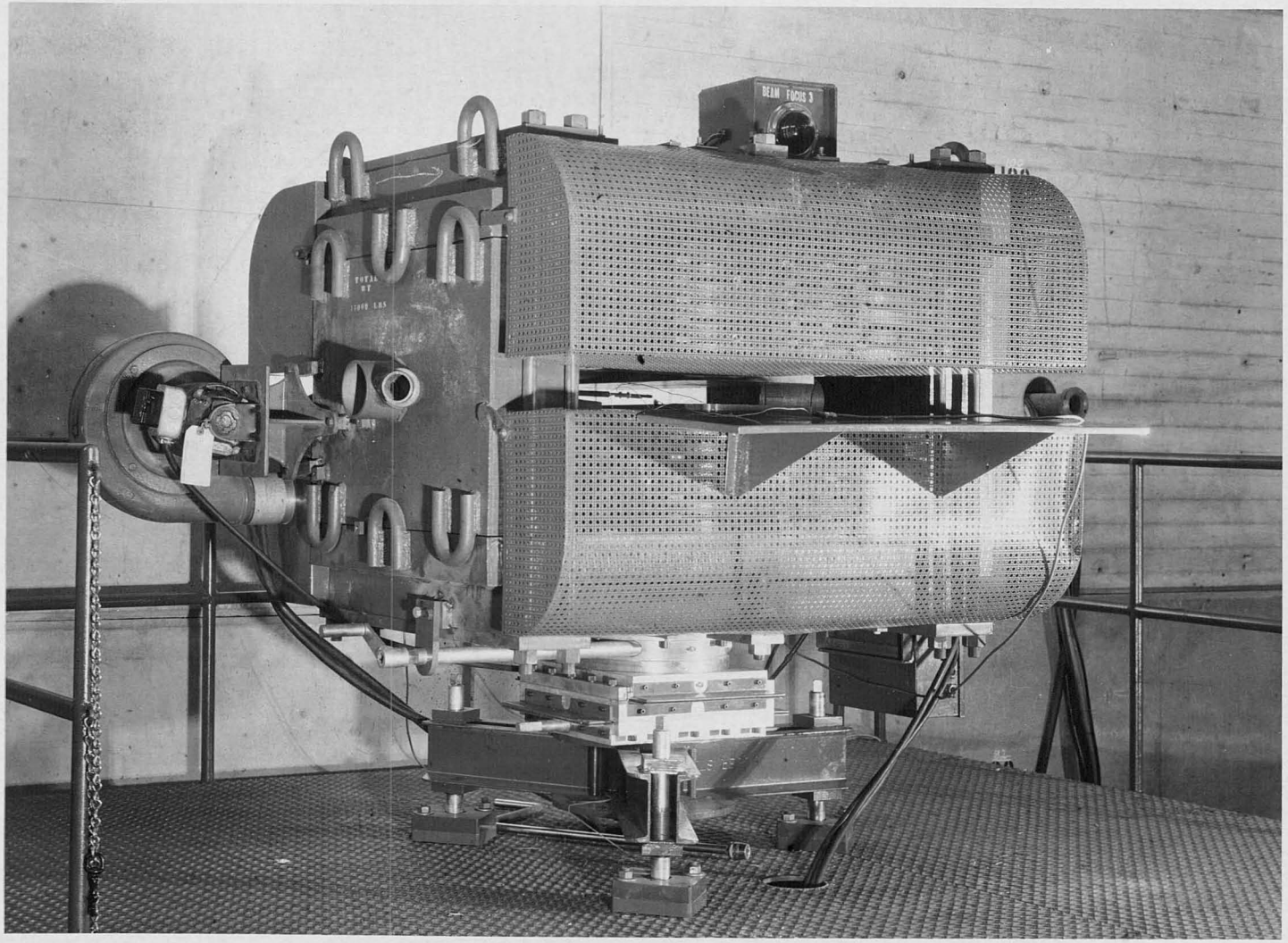

FIG. 42

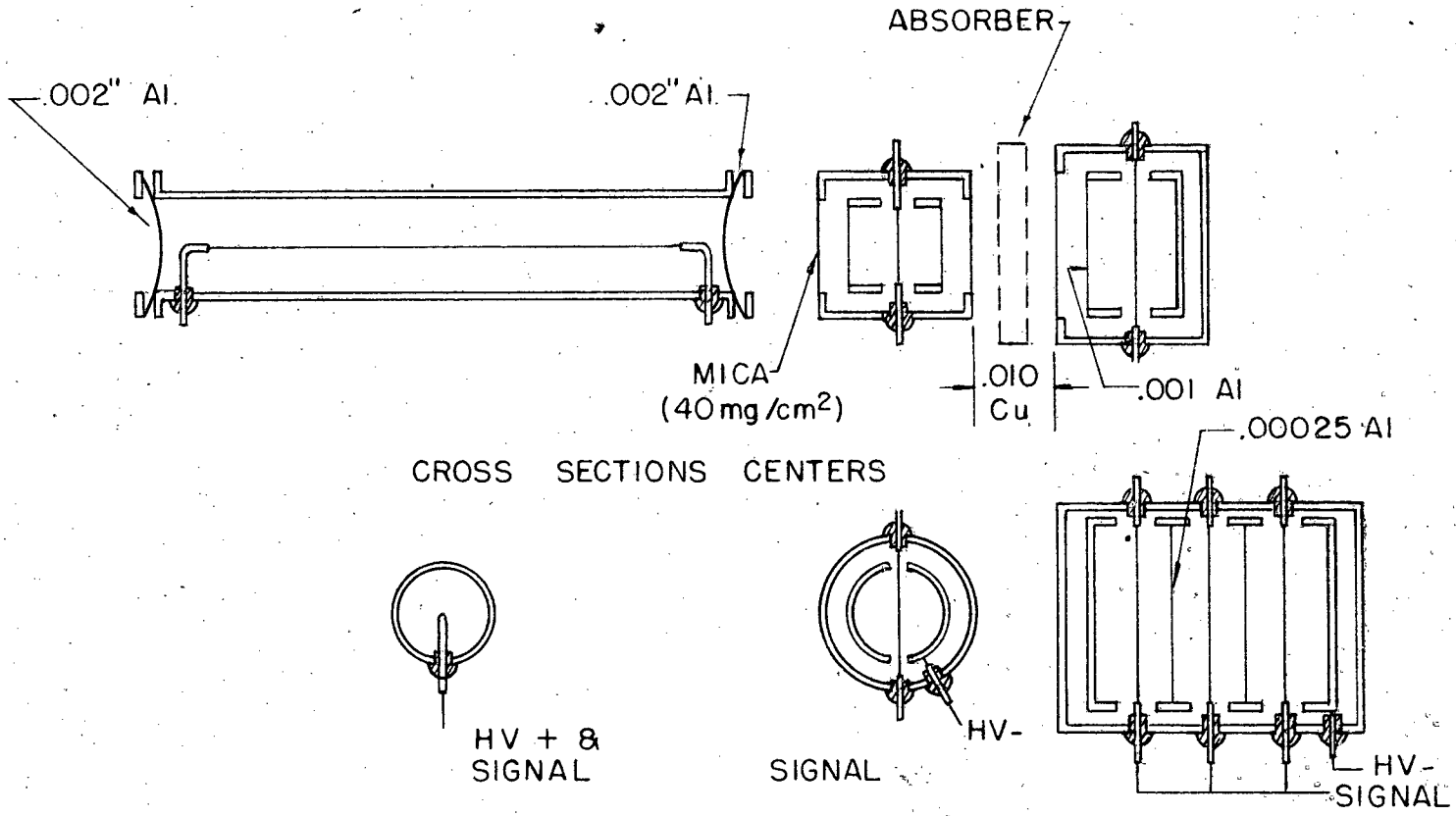

COUNTER TELESCOPE

FIG IV - 3

width of about six percent of its value, plus a low energy tail. The tail is presumably due to alphas which hit the walls of the counter before stopping or which have suffered scattering collisions in the filling tube. The pulse height distribution obtained in the case where the alphas travelled parallel to the axis was essentially the same as that shown.

The Po source consisted of a small amount of polonium plated out on a silver sphere, and was supplied by Dr. Robert Leininger.

The requirements placed on the second and third counters of the telescope are not as stringent as those on the first; they are required only to be able to detect the particles of interest. They each consist of two brass shells, with windows as shown, and with an anode wire passing through the inner one. The outer shell is the gas envelope, and the inner shell is the high voltage electrode. The wires are supported, as in the case of the first tube, by means of a kovar seal arrangement, and are essentially at ground potential (actually at the potential of the grid of the first tube of the preamplifier).

The third tube has been constructed so as to have a large area (4" x 4") in the plane perpendicular to the axis of the telescope. The large area is helpful in preventing the loss of particles which may undergo small angle scattering in the absorber which is placed in front of this tube in some of the procedures to be discussed. In order to have both a fast collection time and a large area it is necessary to

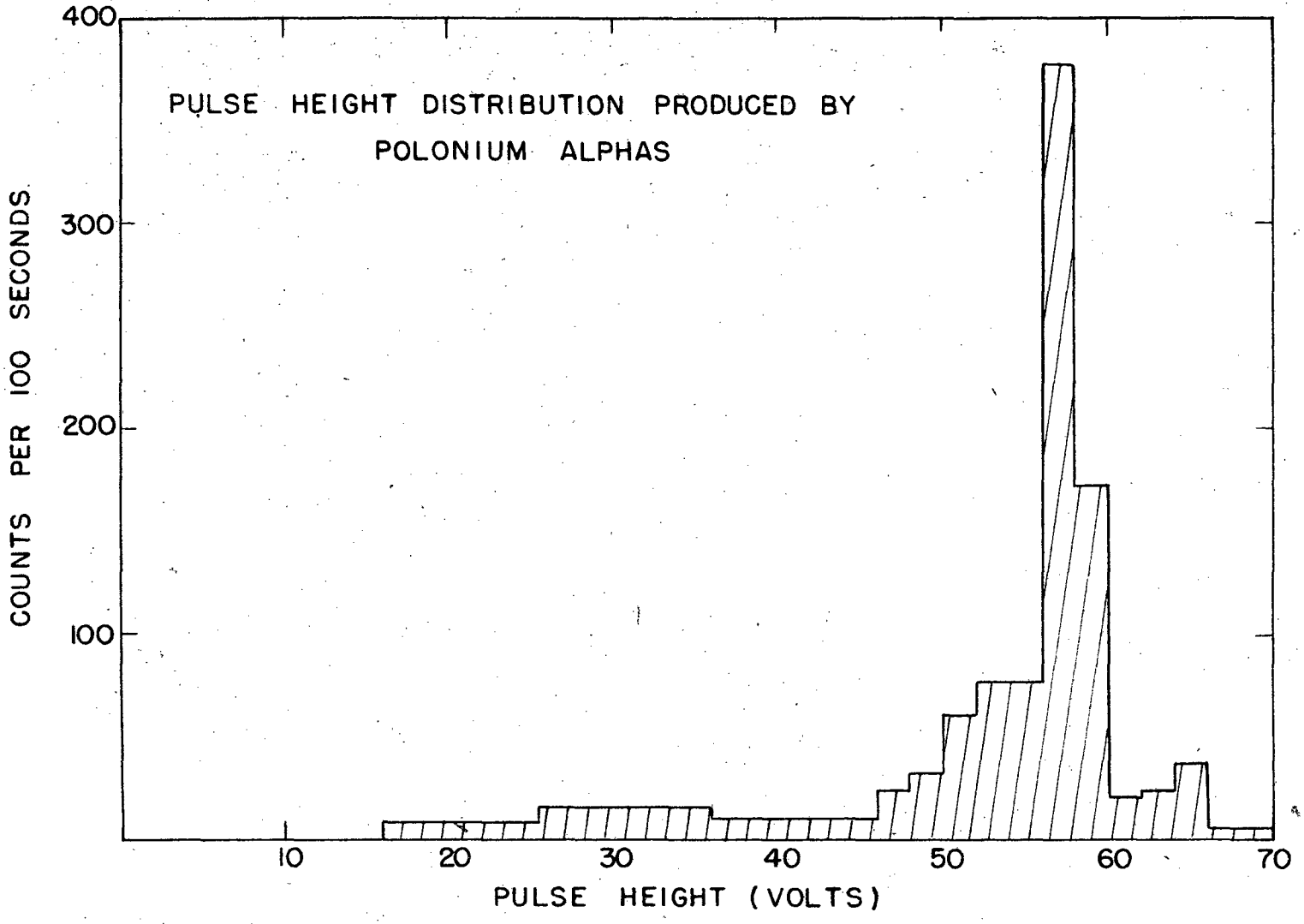
PULSE HEIGHT DISTRIBUTION PRODUCED BY
POLONIUM ALPHAS
COUNTS PER 100 SECONDS
400
300
200
100
10
20
30
40
50
60
70
PULSE HEIGHT (VOLTS)

FIG IV-4

place three parallel collecting wires in the tube in such a way that all particles pass within at most two cm of some collecting electrode. Thin (1/4 mil) sheets of dural are placed between the wires and at high negative voltage with respect to them, so that there are high electric fields at all points in the counter.

E. Electronics

The electronic equipment consists of two parts: a set of amplifiers, preamplifiers, and coincidence gate forming units built by the Electronics Group under the direction of H. Farnsworth, and a pulse height analysing system designed by Dexter and Sands[13] at the Los Alamos Scientific Laboratory, and built, with some modifications, by W. Goldsworthy and Clyde Wiegand at the Radiation Laboratory. A block diagram of the system is shown in Figure IV-5.

The output of each of the three counters is treated alike at first, in each case the signal is fed into a preamplifier which has a gain of about 20, and then to the main amplifier, which has a variable gain ranging between about 1000 and 16,000. Each of the pulses from the first counter then is divided into two parts, one of which goes to the delay unit, shown at the bottom of the diagram, where it is held up for about 10 microseconds, thence to the register pulse generator, and thence, neglecting for the moment the box marked "coincidence unit", to each of the scalers shown connected to the pulse height analyser. Only one of these scalers fires however, which one being determined by what happened

to the other part of the pulse. This other part of the pulse, whose height is determined by the ionizing event causing it and the overall amplification it has received, goes into the pulse height analyzer. The analyzer consists of eleven channels, each of which responds only to pulses having pulse heights within a certain range. When one of these channels responds to a certain pulse, it readies the scaler opposite, and only that scaler will record the register pulse mentioned above. The analyzer is designed so that there is a wide choice of the pulse heights to which a given channel is sensitive. The range of the channels may be either two, five or ten volts, each channel covering a range immediately adjacent to that of its nearest neighbors. When the channel widths are five volts, the lowest channel can be set to count pulses with heights greater than any multiple of five volts, from five to one hundred and twenty-five. A similar situation holds for the case of two volt channels and ten volt channels. A pulse height generator which puts out pulses whose heights vary linearly with time is provided with the unit, and is used to calibrate the channel positions.

The pulses from the other two counters follow two identical paths. Each is delayed in the "delay unit" for ten microseconds, and then fed into the "gate forming unit" which produces uniform square pulses four microseconds in length. These are then fed into the "coincidence unit." Only if these two gates arrive at the coincidence unit at the same time as the register pulse can the register pulse pass through this unit and on

into the scalers.

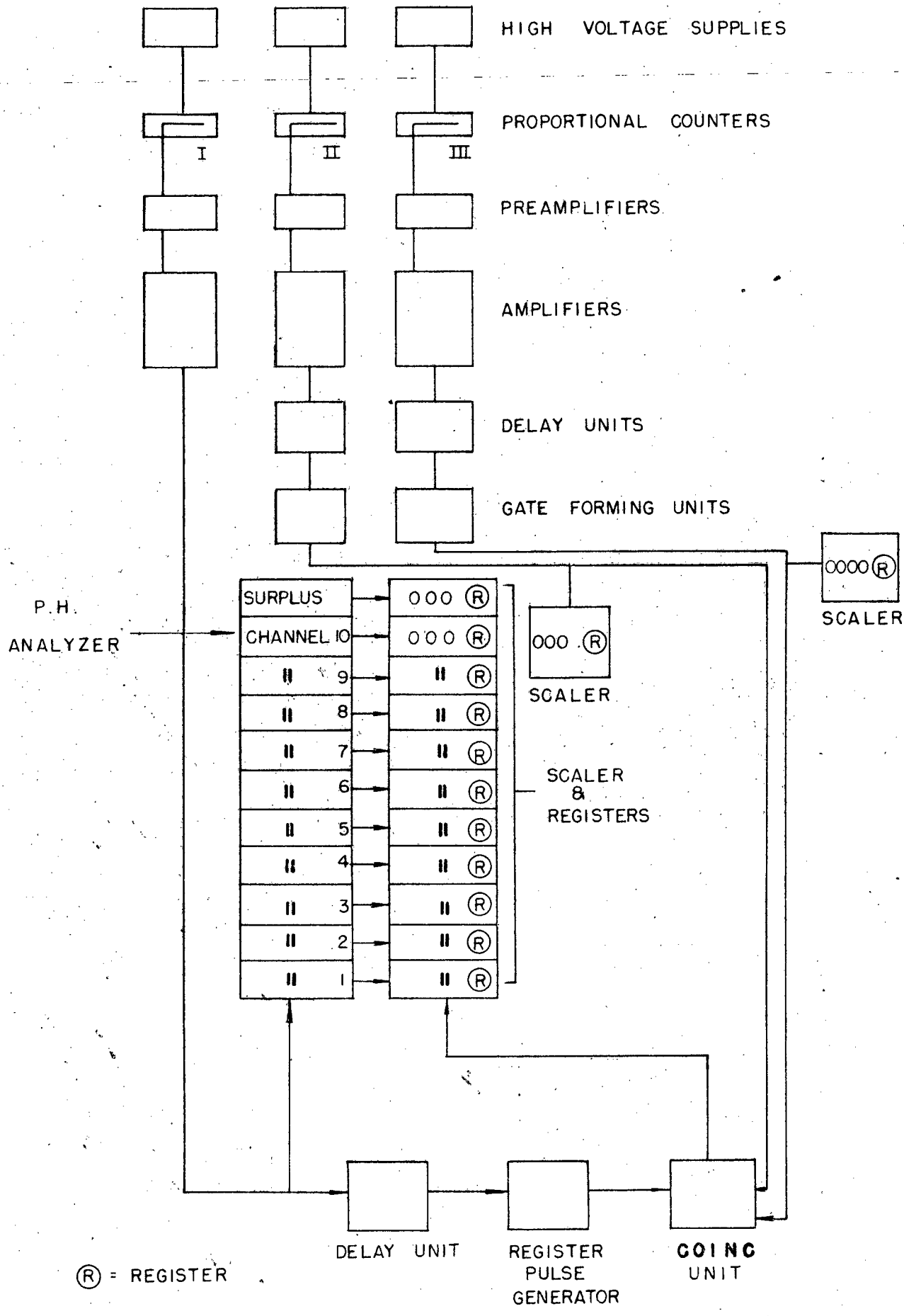

FIG IV - 5

13681-1

V. DETAILS OF MEASUREMENT, $H\rho$-SPECIFIC IONIZATION METHOD

A. Primary Adjustments and Typical Set of Data

As an example, let us consider the measurements made with a scattering angle $\theta = 0^{0}$, a field of 7400 gauss and a ρ of 60". With these values of H and ρ the particles being detected should be protons of about 63 Mev, and deuterons of about 31 Mev. In order to adjust the overall gain of the counting system (electronic gain times gas multiplication) a 1/4" polyethylene, $(CH_2)_n$, scatterer is first set in the position normally occupied by the C, Cu, or Pb scatterers. It is known from n-p scattering experiments that in this energy range the number of particles coming from n-p collisions, all of which must be protons, is considerably greater than the number coming from n-C interactions. The pulse height analyzer is adjusted so that the channels are five volts wide, beginning at five volts, and then the overall pulse amplification is adjusted so that most of the counts from this scatterer come near the bottom of the pulse analyzer, say the second or third channel. Under these conditions an additional small group of counts, caused by deuterons, will be found near the top of the analyzer. That the principal peak really consists of protons rather than deuterons is checked by replacing the $(CH_2)_n$ with a scatterer containing an equal mass of carbon and observing the large decrease in the number of counts making up the principal group, while the other group does not change. The identity of the particles may also be checked by comparing the pulse height of these particles to the pulse heights produced by the polonium alpha source which

the counter contains.

Figure V-1a shows the pulse height distribution obtained in a 300 second run using a 1/8" carbon scatterer (solid curve) with the system adjusted as just described, and the distribution obtained with no scatterer in place for the same length of time (the beam monitoring system will be described later). Figure V-1b then shows the difference between these two and is thus the pulse height distribution for the particles originating in the carbon. Actually, these data were obtained in two steps, since the range in pulse heights shown is greater than the range of the pulse height analyser. The lower part of the distribution was obtained with the pulse height analyser set to measure pulses having heights between 5-55 volts, and the upper part with the analyser working in the range of 30-80 volts. The number of pulses found above 55 volts in the second case, all of which are ascribable to deuterons, checked with the number in the surplus channel in the first case.

It can be seen that the pulses fall into two groups, the lower of which is known to consist of proton pulses, for the reasons given above. The other group is seen to have an average pulse height three times as great as the lower group and therefore consists of deuteron pulses. A further check on these classifications has been made by making the following absorption experiment. A carbon absorber whose thickness is equal to the range of a 45 Mev deuteron (and hence a 34 Mev proton) was placed between the second and third counters. It was then observed that the

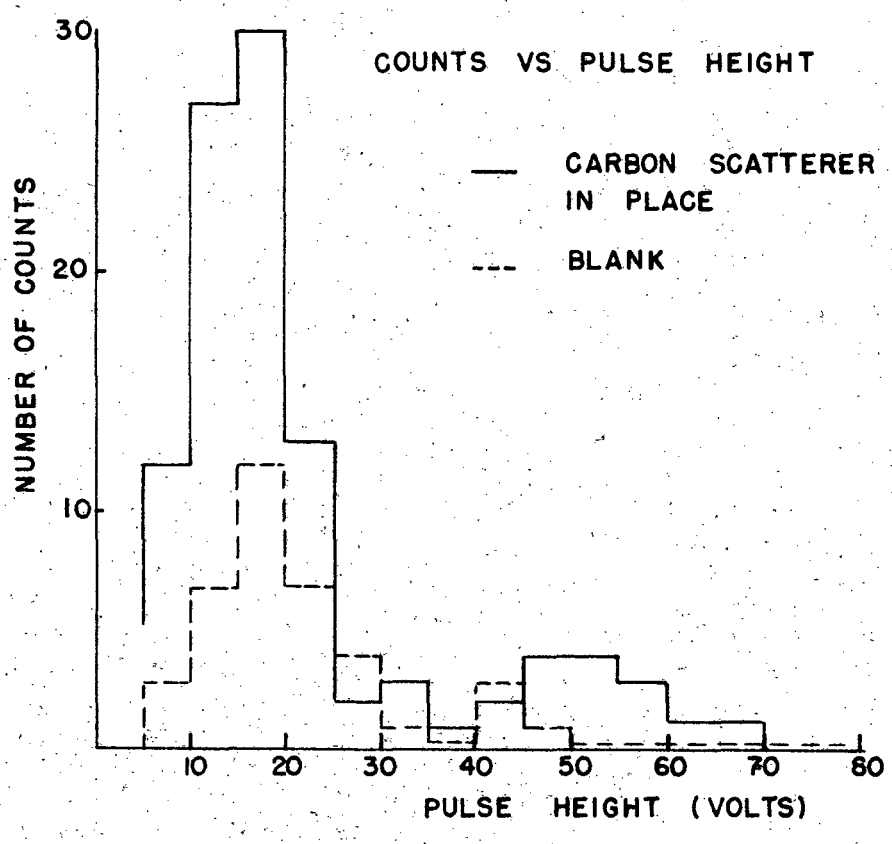

FIG V - 1a

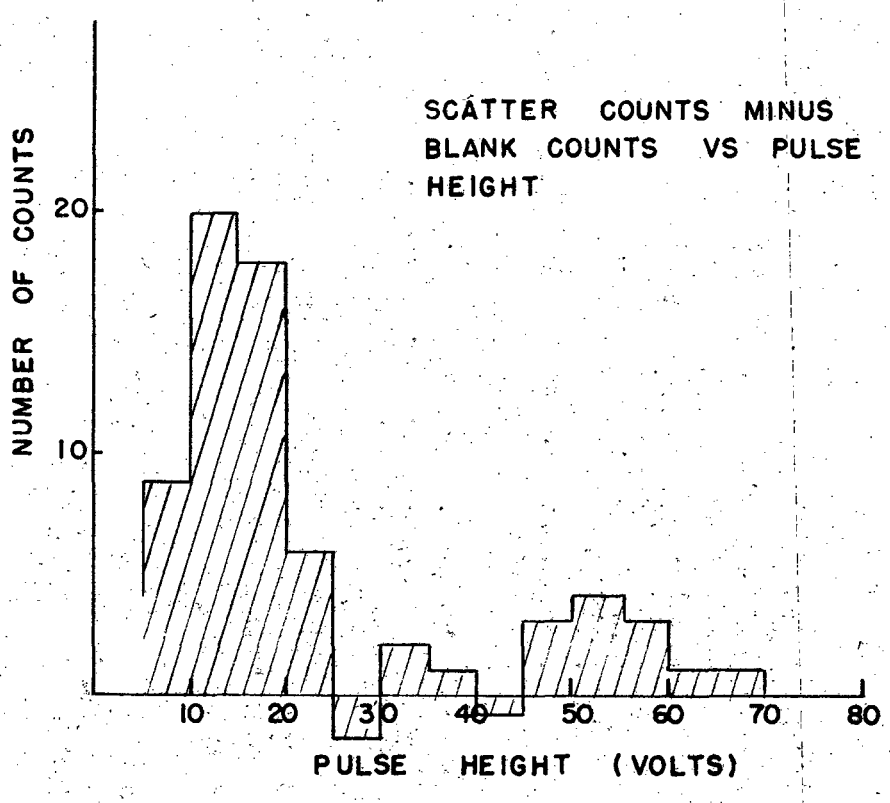

FIG V - 1b

upper peak disappeared entirely, while the lower peak was unaffected within the statistics. This check was used in a number of instances when one of the peaks was so small its origin was somewhat doubtful, as in the case of the very small number of tritons found at high values of magnetic field.

The background count decreases relative to the total count as the scattering angle increases. For example, relative to the total count with the 1/8" C scatterer in place, the ratio of background to total is .35 at 0°, .20 at 12°, .10 at 25° and .07 at 45°. The background consists chiefly of charged particles produced in the air column traversed by the beam, and which travel along a path such that they can enter the magnet and pass thru the slit and counter system. The length of the contributing air column obviously becomes much shorter as the angle of observation increases. The lead brick placed just to the right of the scatterer as shown in Figure III-1 helps to reduce the background by cutting out a number of possible paths of background particles. However, it is not effective when the angle of observation is 0°, since then most of the possible paths for background particles pass through the region of the scatterer where it is clearly impossible to stop them. At 25° the background with the brick out is about five times larger than with it in.

The individual counting rates of the various counters at the time the data in Figure V-1a were taken were as follows:

Pulses from first tube more than five volts high -- 11/sec.

Pulses from second tube of sufficient height to make make coincidence gates (5 volts) - - - - - - - - 35/sec.

Pulses from third tube of sufficient height to make coincidence gates (5 volts) - - - - - - - - 70/sec.

B. Monitor

Since the neutron beam fluctuates somewhat, it is necessary to have a monitoring system. The system used here is one which has been tested and used by a number of experimenters at the Radiation Laboratory, principally by A. Bratenahl, R. Hildebrand, C. Leith, and E. J. Meyer. It consists of a BF_3 filled proportional counter which is inserted into the concrete cyclotron shielding a few inches away from the high energy neutron collimating hole. The hole into which it is inserted is in fact an additional collimating hole pointed at a different part of the cyclotron. The inner end of this second hole was plugged during these experiments with a six foot brass cylinder. Although the counter itself is, of course, sensitive principally only to slow neutrons, it monitors the fast neutron beam in the following way. Most of the fast neutrons which come through the hole through the shielding strike the steel collimator placed in the outer end of the hole. They are inelastically scattered there and produce in addition a number of secondary neutrons, which are then moderated by the concrete, and become slow neutrons. Some of these find their way to the BF_3 counter and are then recorded. In most of the runs two

such counters were used, one simply serving as a check to show that the sensitivity of the other had not changed.

C. Complete Set of Data Taken at 0° with 1 /8" C Scatterer

Figure V-2 shows a complete set of data of the type in Figure V-1 for a series of different values of magnetic field. The first graph shows the distribution obtained using a field of 4470 gauss. The duration of the run was 300 seconds, as in all the succeeding cases, for both the "scatterer in" count, and the background count. The monitor during this time recorded 175 x 64 slow neutron counts. At this value of magnetic field only one group of particles is seen, corresponding to 23 Mev protons. The 11.5 Mev deuterons which would have the same $H\rho$ are not able to penetrate all of the absorbing material along their potential path, such as the air, and the counter windows. The next and succeeding graphs show the distributions obtained at the indicated values of H . The monitor count recorded during each run is also shown. The graphs are arranged in order of increasing H and therefore increasing energy of the particles. The proton peak can be seen moving steadily to lower values of pulse height since the specific ionization decreases with increasing energy. The first deuteron peak shows up at 6350 gauss and corresponds to a deuteron energy of 23 Mev. At very high magnetic fields the protons are seen to disappear, and a new small peak to the right of the deuterons comes into existence. From its position, and from absorption measurements, this peak is ascribed to tritons.

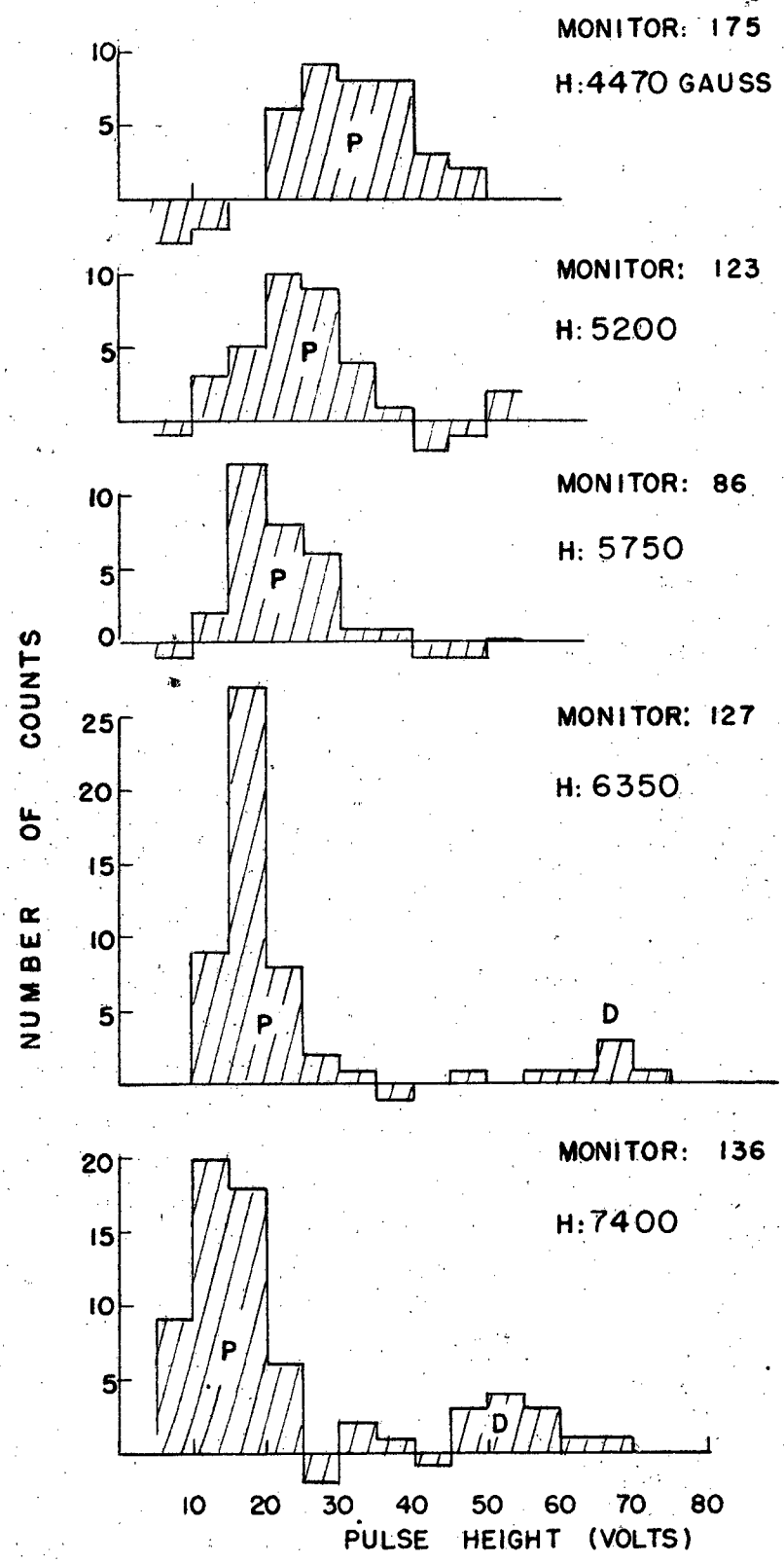

FIG. V - 2

(CONT. ON NEXT PAGE)

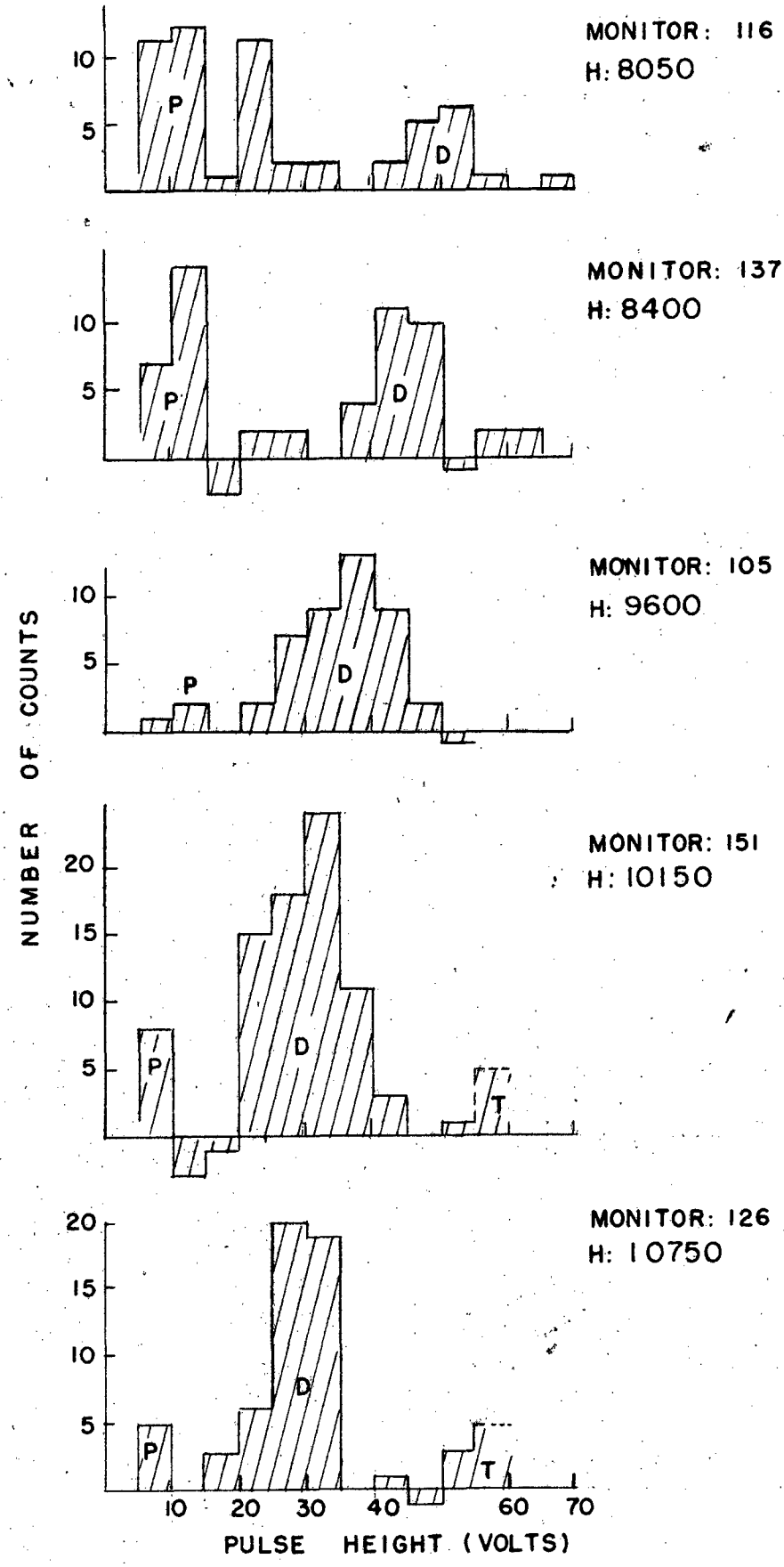

FIG. V - 2 (CONT.)

(CONCLUDED ON NEXT PAGE)

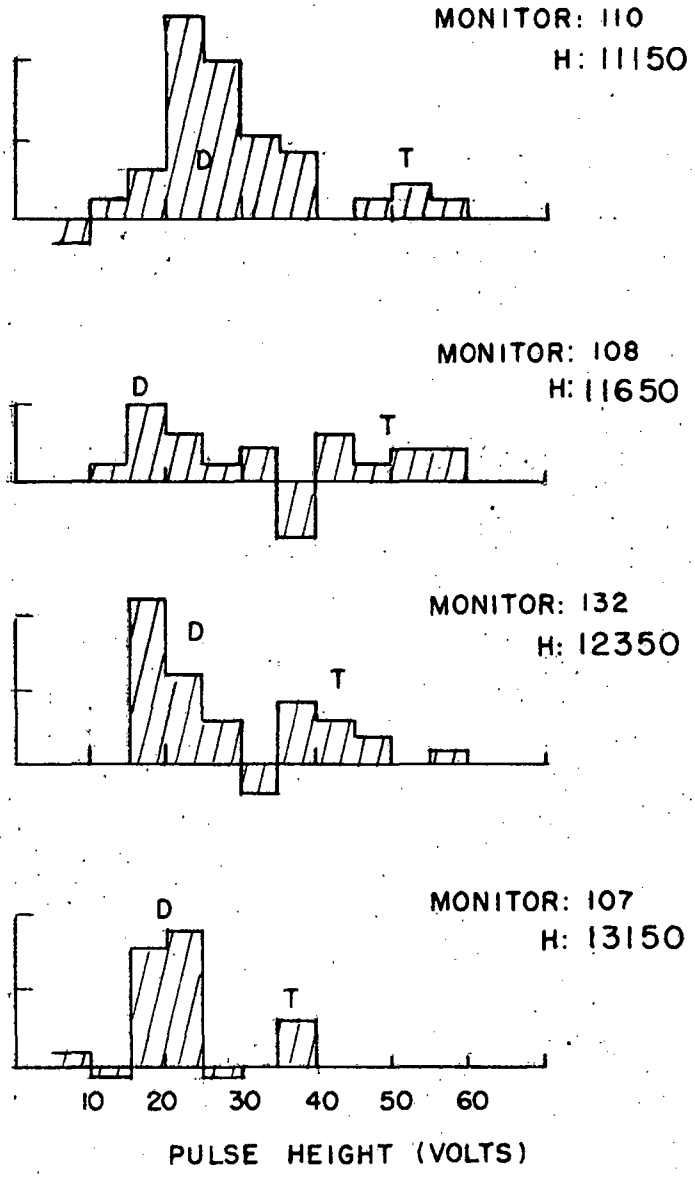
MONITOR: 110
H: 11150
D
T
MONITOR: 108
H: 11650
D
T
MONITOR: 132
H: 12350
D
T
MONITOR: 107
H: 13150
D
T
10
20
30
40
50
60
PULSE HEIGHT (VOLTS)

FIG. V - 2

VI. DETAIL OF H/ρ-RANGE METHOD

A. Experimental Arrangement

The magnet, scatterer, and slit system is set up as in the H/ρ-specific ionization method. The counter telescope is physically the same as before, but the pulses generated there are treated differently, no pulse height analyzer being used. The absorber between the second and last counters is an essential part of the equipment, its thickness being essentially the "range" in question.

B. Desensitization Method

The desensitization method is a scheme for detecting particles whose ranges lie between R and R $+\Delta$ R, where both R and ΔR may have any predetermined values. Using the counter telescope arrangement described above, R is determined simply by the absorber between the last two tubes, taking into account, of course, all other absorbing material in the telescope. ΔR is determined by the sensitivity of the last counter, as can be seen in the following considerations. Suppose the overall amplification (gas multiplication and electronic gain) of the last counter and its associated amplifier is adjusted so that only pulses with a height greater than V_{min} can be detected. V_{min} will, of course, be proportional to the specific ionization of the particle in question times the length of its path in the counter. In the application considered here, the number of particles which actually stop in the last tube is completely negligible, and we will therefore assume that all particles have the same path length in the

counter. Hence, only those particles with a specific ionization greater than some minimum, say I_o, can be counted. The relation between the residual range of a particle, in this case the ΔR above, and its specific ionization was found in Section II-B.

$$\Delta R = a \frac{q^{2.5} m}{I^{2.25}} = b \frac{q^{2.5} m}{V_{min}^{2.25}}$$

where a is independent of the properties and energy of the particle, depending only on the absorber material and the gas in the counter, and b depends in addition on the overall amplification. That part of b which depends on the gas in the counter and the overall amplification was found by comparing the particle pulses to pulses produced by alphas from a polonium source placed in the counter, and that part of b which depends on the absorbing material, in terms of which we wish to express ΔR, were found by consulting the appropriate curves in the Collection of Range Energy Curves compiled by Aron et al[17] using the well known Bethe range-energy relation.

In the use to which this method is put here, it is not necessary to know what ΔR is precisely; the only requirement being that ΔR be much smaller than R.

C. Experimental Procedure

As an example, let us consider the case wherein the apparatus was set up so as to observe particles leaving the scatterer at an angle of 10^0 with respect to the direction of the neutron beam, and having a mean

radius of curvature of 60" in the magnetic field. With the slit system used, the spread in the accepted radii of curvature was about 60 $\pm$ 10 inches. The absorber was a 2.0 gm/cm^2 C slab, so that R corresponded to an energy of 48 Mev in the case of protons, and an energy of 65 Mev in the case of deuterons. The sensitivity of the last counter was adjusted so that R + ΔR corresponded to 52 Mev in the case of protons, and 73 Mev in the case of deuterons. The ratio of the coincidence counts, with and without the carbon scatterer in place, to the monitor counts was then observed as for various magnetic fields.

D. Results

A plot of the ratio of coincidence counts to monitor (with the background count subtracted) as a function of magnetic field, is shown in Figure VI-1. It can be seen that for very low fields, no particles were counted, since neither protons nor deuterons having energies corresponding to these small Hρ's can penetrate the absorber. As the field increases, protons traveling along some of the possible paths begin to have an energy sufficiently large to allow them to penetrate to the last counter, and the ratio of counts to monitor begins to increase. Eventually a condition is reached where the largest number of possible paths through the slit system correspond to protons having ranges between R and R +ΔR. Under this condition, the detected particles are those having a ρ equal to the mean radius of curvature accepted by the slit system, i.e. 60". As the field increases further, more and more of the protons accepted by the slit system

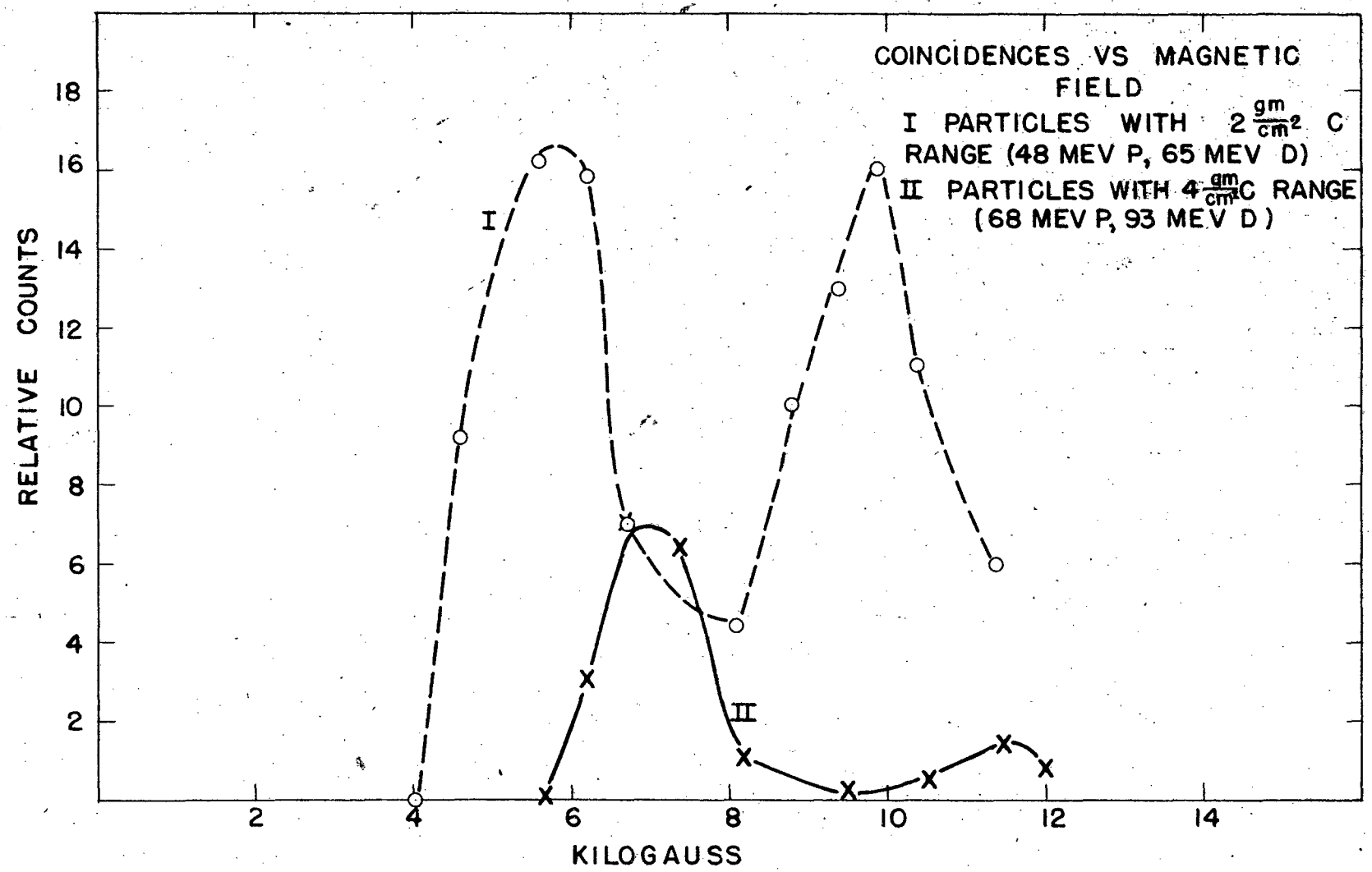
COINCIDENCES VS MAGNETIC FIELD
I PARTICLES WITH 2 gm/cm² C RANGE (48 MEV P, 65 MEV D)
II PARTICLES WITH 4 gm/cm² C RANGE (68 MEV P, 93 MEV D)
RELATIVE COUNTS
KILOGAUSS
I
II
2
4
6
8
10
12
14
16
18

FIG VI - 1

have energies such that they pass undetected through the desensitized counter, and the counting rate decreases. At still higher fields, a condition is reached where the deuterons accepted by the slit system have ranges between R and R $+\Delta$R and another peak similar to the first is observed.

Within the accuracy of this experiment, (the uncertainty in ρ was discussed in Section III-A) the two peaks are seen to correspond indeed to protons and deuterons. For a ρ of 60", and the absorber used, the proton peak should theoretically occur at H = 6400 gauss and the deuteron peak at H = 10400 gauss. Moreover, the ratio between the masses of the particles making the two peaks can be checked with greater certainty, assuming the q's of the particles to be the same, since then the value of ρ does not enter. Taking the two peaks to be at 5800 gauss and 9800 gauss, and using the equations of Section II-B, the ratio of the masses turns out to be 2.07.

Figure VI-1 also shows another curve of the same type obtained for a 4.0 gm/cm^2 carbon absorber, the corresponding proton and deuteron energies in this case were 68 and 93 Mev.

The spread in the radii of curvature accepted by the slit system was made larger in the case of these measurements than in the previous case for the following reason. Both the slit system, which determines ρ within some small range of values characterized by $\Delta\rho$, and the desensitized counter system, which determines R within some small range of R's characterized by ΔR, are systems which can fix the range of energies detected within some range of values ΔE. In order to interpret the results obtained, it is

necessary to have ΔE as fixed by one of these two systems be much smaller than that fixed by the other. Since the ΔE as fixed by the desensitized counter system is much easier to control and determine than the ΔE that can be fixed by the slit system, $\frac{\Delta \rho}{\rho}$ was made deliberately large. $\frac{\Delta \rho}{\rho}$ must, of course, also be small enough to resolve the two peaks shown in Figure VI-1.

The $H\rho$-range method proved to be inferior in several ways to the $H\rho$-specific ionization method, not the least of which was that it takes of the order of five to ten times as long to get the same amount of information. It was therefore not used as a means of getting a detailed picture of the particle knock-out processes, but it does serve as an additional check on the fact that the deuteron yield is of the same order as the proton yield.

VII. ANALYSIS OF DATA

A. Resolution and Calibration of $H\rho$

As mentioned in Section III the final measurement of the ρ of the particles is made by means of the particles themselves. As an example of how this is done, let us consider the measurement of ρ again in the case of the 0° observations described in detail in Section V-A. The magnet current was set at 46 amperes, which gave a field of 6800 gauss. The ratio of proton counts from the carbon scatterer (with the background subtracted out) to the monitor count was then observed. This observation was then repeated with various thicknesses of carbon absorber between the second and third tubes. In this way an attenuation curve of the protons was obtained. By plotting the ratio of proton counts to monitor counts, versus the energy of a proton which can just penetrate the absorber (taking into account absorption by the air and counter windows) we obtain the integral spectrum of protons shown in Figure VII-1a. By differentiating this curve (actually by subtracting the $(n + 1)$ st point from the nth point) a curve, shown in Figure VII-1b, is obtained which is the energy distribution of the protons which are accepted by the slit system at this magnetic field. The mean energy in this case is seen to be 52.5 Mev, with slightly less than one-half of the particles falling between 50 and 55 Mev. ρ is thus found to be 60.5 inches as compared with the geometrical value of 60 inches.

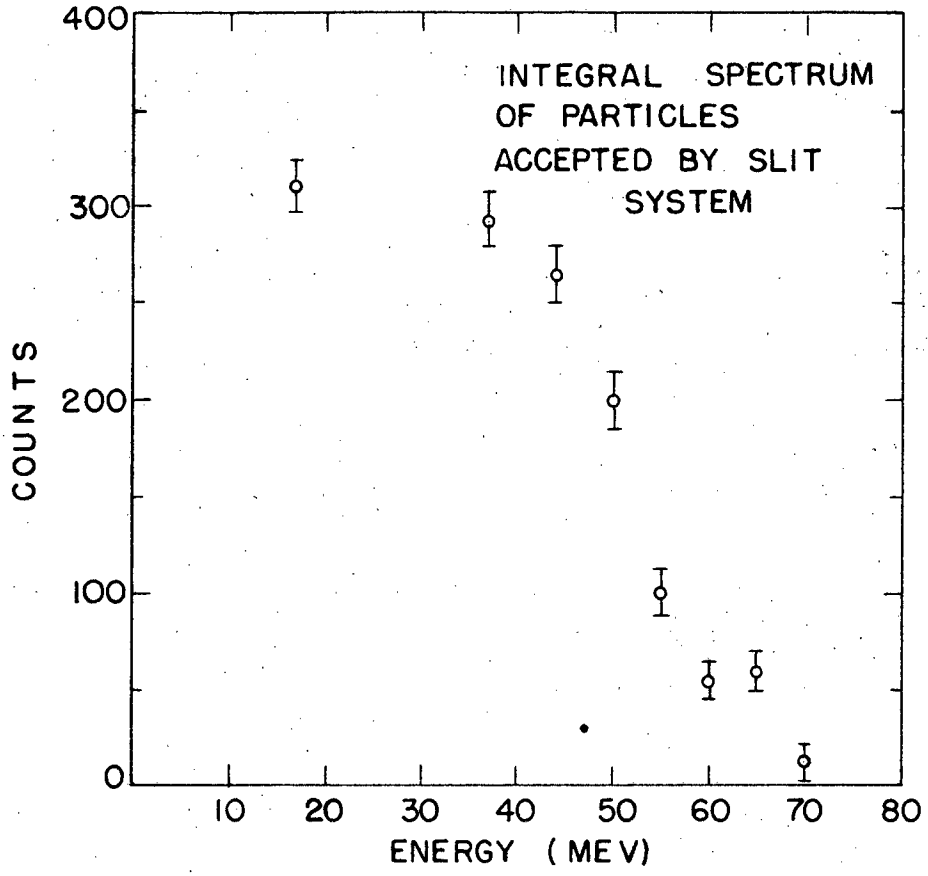

FIG VII - 1a

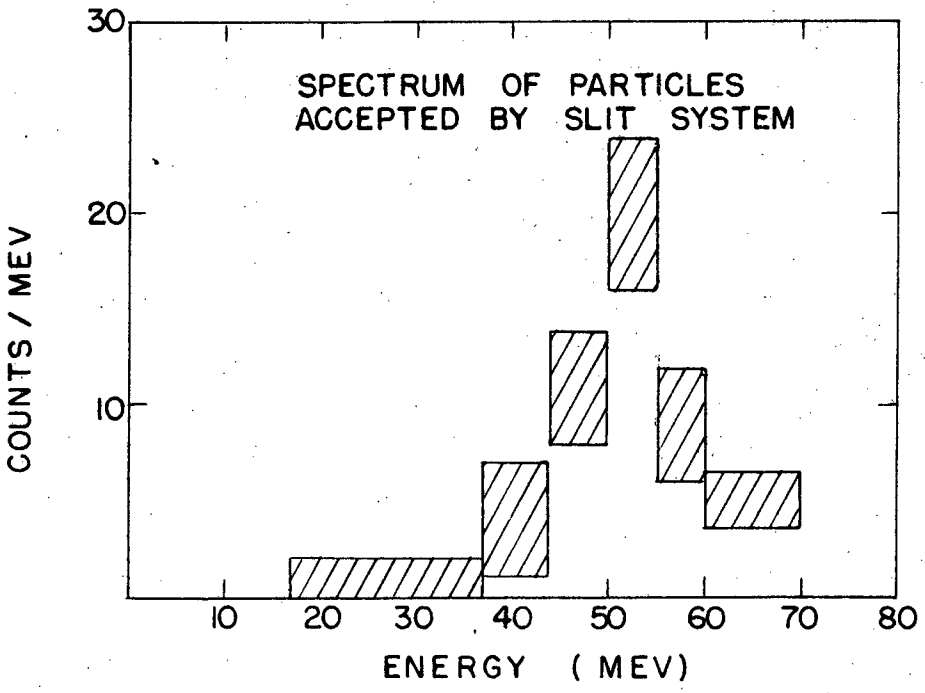

FIG VII - 1b

B. Definition of Terms

The ultimate goal of this experiment is to determine the differential cross section for the production of secondary charged particles of energy E at an angle θ. We shall define this quantity as $\frac{d\sigma_p(\theta, E)}{d\Omega\, dE}$ (abbreviated in the text by $d\sigma_p$) where the subscript p stands for protons and d and t will stand for deuterons and tritons. The units of this quantity will be millibarns ($10^{-27}cm^2$) per steradian per Mev. Because of the finite resolving power of the slit system, this quantity is not measured at a single energy, but its average value between two limits E_ℓ (lower energy limit) and E_u (upper energy limit) is the quantity which is found. In the following discussion, the above symbol will also be used to express its average value between these two energies. We shall first take up the absolute determination of E_ℓ and E_u, and the relative determination of $d\sigma_p$, and then later describe the methods by which the absolute value of $d\sigma_p$ is found.

In the following we shall call the mean energy of the particles accepted by the magnet E_m, and ΔE_m will characterize the width of the energy distribution of the accepted particles.

C. Reduction of Data for the Case of an Infinitely Thin Scatterer

For simplicity, let us take for the spectrum of accepted particles a rectangular step function of width E_m - 6 Mev centered at E_m - 52 Mev. Then, since there is a $\frac{\Delta\rho}{\rho}$ related to $\frac{\Delta E_m}{E_m}$ $\left(\frac{\Delta E_m}{E_m} = 2\frac{\Delta\rho}{\rho} \text{ for small } \frac{\Delta E_m}{E_m}\right)$, and since $\frac{\Delta\rho}{\rho}$ depends only on the geometry, $\frac{\Delta E_m}{E_m}$ is a constant independent of

energy. Therefore, to get the relative spectra of the particles at each angle, we have merely to divide the relative counting rate observed at each magnetic field by E_m:

$$\left(\frac{d\sigma_p(\theta,E)}{d\Omega\, dE}\right)_{\text{relative}} = \frac{N_p(\theta,E_m)}{(Mon)E_m}$$

Where $N_p(\theta,E_m)$ is the number of protons counted, (Mon) is the monitor count. Also we have the following obvious relations for the limits of the energy range to which this $d\sigma_p$ pertains:

D. $$E_l = E_m - \frac{\Delta E_m}{2}$$
$$E_a = E_m + \frac{\Delta E_m}{2}$$

D. <u>Reduction of Data for a Scatterer of Finite Thickness</u>

Here the situation is considerably more complicated. We shall first take up the determination of $d\sigma_p$ ($d\sigma_d$ and $d\sigma_t$ being determined in the same way). Consider a scatterer of thickness T as shown in Figure VII-2. Protons originating in the interval dt at t must have energies between $E_1(t)$ and $E_2(t)$, where $E_1(t)$ is such that the proton will have an energy $E_m - \frac{\Delta E_m}{2}$ when it reaches t = 0, and $E_2(t)$ is such that the proton will have an energy $E_m + \frac{\Delta E_m}{2}$. If we now define $\Delta E(t)$ as $E_2(t) - E_1(t)$ we can express $d\sigma_p$ as follows:

$$\left(\frac{d\sigma_p(E,\theta)}{d\Omega\, dE}\right)_{rel} = \frac{N_p(\theta,E_m)}{(Mon)\ \overline{\Delta E(T)}}$$

where $\overline{\Delta E(T)}$ is the average value of $\Delta E(t)$ between t = 0 and t = T.

If we introduce the quantities r_a and r_b such that r_a is the range

of a proton of energy $E_m = \frac{\Delta E_m}{2}$ in the scatterer material, and r_b is related in the same way to $E_m + \frac{\Delta E_m}{2}$, we may write

$$E_1(t) = E(\Lambda_a + t)$$
$$E_2(t) = E(\Lambda_b + t)$$

where the symbols on the right stand for the energy of protons having the range in the parentheses. Hence,

$$\Delta E(t) = E(\Lambda_b + t) - E(\Lambda_a + t)$$

To find $\Delta E(t)$ then, we may make a graphical analysis using the Collection of Range-Energy Curves, prepared by Aron et al[17] using the Bethe range-energy relation. It may also be found by algebraic means using the previously quoted empirical relation between range and energy. The first method is the most accurate in principle, but, because of the difficulty of reading the graphs well enough to determine the small differences involved, the second is much more accurate in practice, and is the method used here.

For the empirical relation we take as before:

$$R = kE^c$$

where k depends on the charge, and mass of the particle in question, and also on the material it is penetrating, and c is an empirically determined number, equal to 1.6 in the energy range of interest here.

We then obtain

$$\Delta E(t) = \left(\frac{\Lambda_b + t}{k}\right)^{1/c} - \left(\frac{\Lambda_a + t}{k}\right)^{1/c}$$

and hence

$$\Delta E(t) = \left(\frac{\Lambda_a}{k}\right)^{1/c}\left[\left(\frac{\Lambda_b}{\Lambda_a} + \frac{t}{\Lambda_a}\right)^{1/c} - \left(1 + \frac{t}{\Lambda_a}\right)^{1/c}\right]$$

and since $E_m - \frac{\Delta E_m}{2} = E_1(0)$

$$\Delta E(t) = E_1(0)\left[\left(\left[1+\frac{\Delta E_m}{E_m}\right]^c + \frac{t}{\lambda_a}\right)^{1/c} - \left(1+\frac{t}{\lambda_a}\right)^{1/c}\right]$$

Figure VI-2 gives a plot of the ratio $\frac{\Delta E(\frac{t}{\lambda_a})}{\Delta E_m}$ vs (t/r_a), calculated for $\frac{\Delta E_m}{E_m} = .12$, and also of the average of this quantity between $t = 0$ and $t = T$, again as a function of (T/r_a). This average value is denoted as y, and is the quantity of direct interest. y is very insensitive to the value of $\frac{\Delta E_m}{E_m}$; values of y calculated for this latter ratio taken as .2 instead of .12 differ by only 3% in the worst case, which occurs for $T/r_a \gg 1$. This means that y, and hence the calculation of the spectrum, is quite insensitive to the shape of the magnet acceptance curve in Figure VII-1.

In terms of y, $d\sigma_p$ may be written:

$$\left(\frac{d\sigma_p(\theta,E)}{d\Omega\, dE}\right)_{\text{absolute}} = k\,\frac{N_p(\theta,E_m)}{(M_{on})\, y\, \Delta E_m}$$

where k is independent of E_m and, for the nonce, undetermined. Values of y as a function of E_m are given in Figure VII-3 for the various scatterers used, and for protons and deuterons in each case.

As mentioned above, this $d\sigma_p$ is an average value over a certain range of energies. We shall now take up the question of what the energy limits of this range are. To do this, we shall consider three different cases: $T > r_b - r_a$, $T = r_b - r_a$, $T < r_b - r_a$, and we shall again assume that the slit system accepts no particles having energies below $E_m - \frac{\Delta E_m}{2}$ or above $E_m + \frac{\Delta E_m}{2}$, and accepts all particles within this range equally well.

Case I, $T > r_b - r_a$

Let us call the energy, with which the particle leaves the nucleus, E, and let us plot the thickness, Δt, of the scatterer from which particles

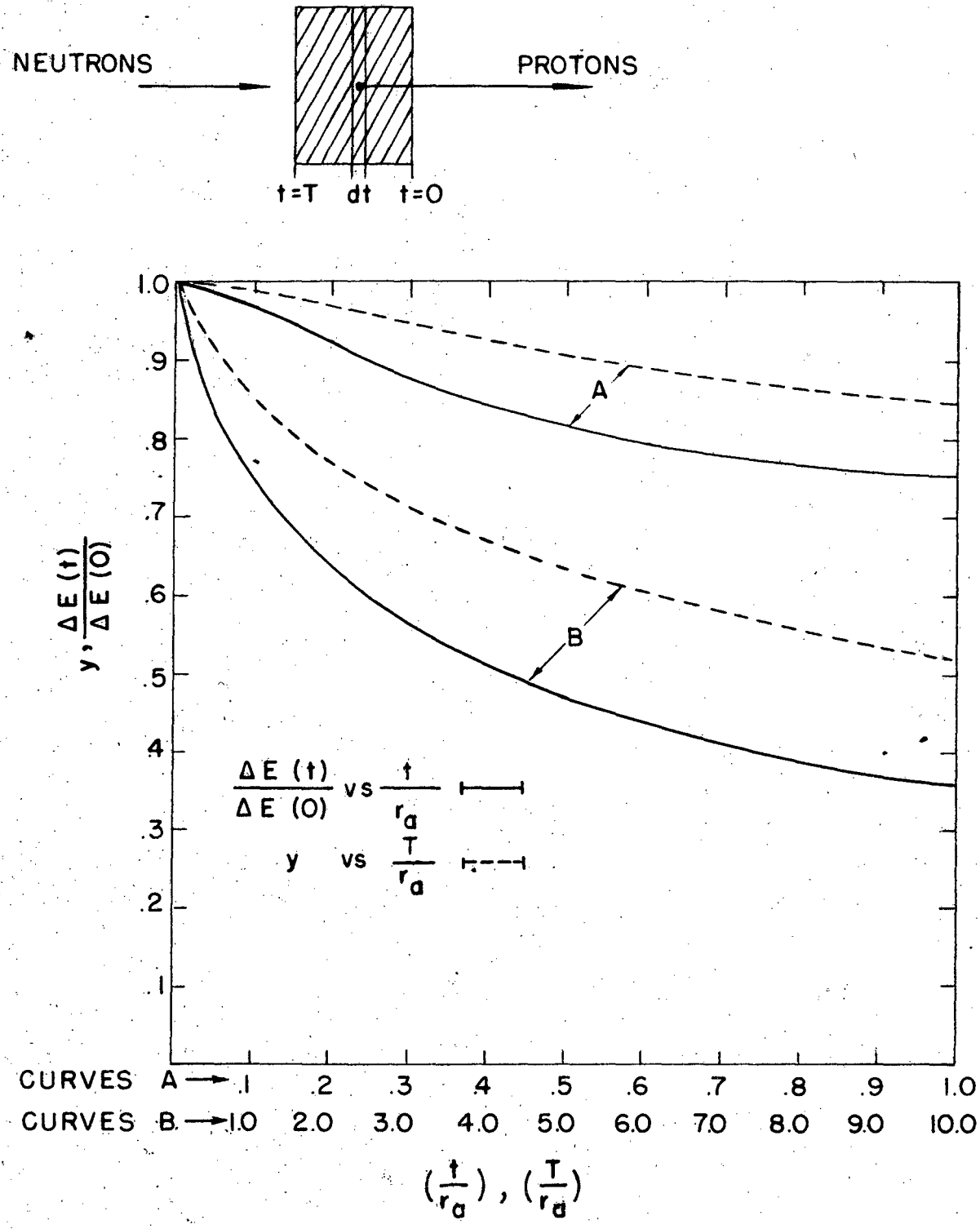
NEUTRONS
PROTONS
t=T
dt
t=0
1.0
.9
.8
.7
.6
.5
.4
.3
.2
.1
y, ΔE (t) / ΔE (0)
A
B
ΔE (t) / ΔE (0) vs t / r_a
y vs T / r_a
CURVES A → .1 .2 .3 .4 .5 .6 .7 .8 .9 1.0
CURVES B → 1.0 2.0 3.0 4.0 5.0 6.0 7.0 8.0 9.0 10.0
(t / r_a) , (T / r_a)

FIG VII - 2

of energy E can be detected. A diagram of the scatterer and the plot of Δt vs E are shown in Figure VII-4. For $E<E_m = \frac{\Delta E_m}{2} = E(r_a)$ no part of the scatterer contributes. For $E = E(r_a)$, only the infinitely thin layer at $t = 0$ can contribute. For $E = E(r_b)$, that part of the scatterer lying between $t = 0$, and $t = r_b - r_a$ can contribute particles. This same thickness, $r_b - r_a$, will contribute in the case of all particles with energies between $E(r_b)$ and $E(T - r_a)$, since, if R is the total range of a particle within this energy interval, the part of the scatterer which can contribute is that between $t = R - r_a$ and $t = R - r_b$, so $\Delta t = r_b - r_a$. As E increases above $E(T + r_a)$, Δt decreases, becoming zero again at $E(T + r_b)$. In view of the shape of this curve, the end points of the range of the measurement made under these conditions is somewhat arbitrary, becoming more so as $T \to \Lambda_b - \Lambda_a$. However, a reasonable choice of the end points, for the purpose of deciding where to plot $d\sigma_p$, would seem to be:

$$E_\ell = \frac{E(\Lambda_a) + E(\Lambda_b)}{2} = E_m$$

and

$$E_u = \frac{E(\Lambda_a + T) + E(\Lambda_b + T)}{2}$$

In the final plot of $d\sigma_p$ vs E, the "point" $d\sigma_p(E)$ is plotted as a rectangle whose end points in the direction of the E axis are E_ℓ and E_u, and whose height is a measure of the uncertainty in $d\sigma_p$ due to statistics.

Case II, $T = r_b - r_a$

Using the same approach as in Case I, we find that the curve giving Δt

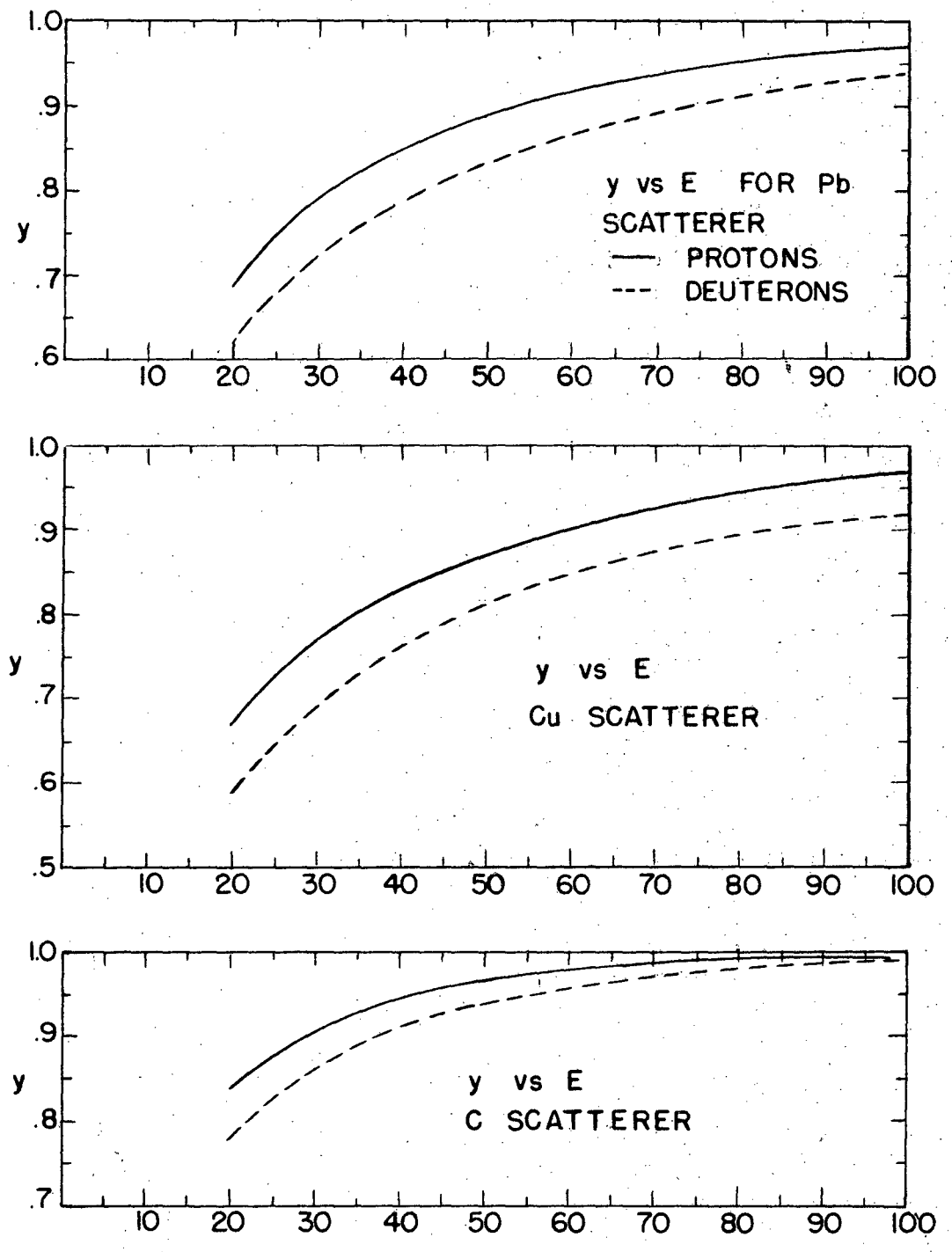
1.0
.9
.8
y
.7
.6
y vs E FOR Pb
SCATTERER
PROTONS
DEUTERONS
10 20 30 40 50 60 70 80 90 100
1.0
.9
.8
y
.7
.6
.5
y vs E
Cu SCATTERER
10 20 30 40 50 60 70 80 90 100
1.0
.9
y
.8
.7
y vs E
C SCATTERER
10 20 30 40 50 60 70 80 90 100

FIG VII - 3

as a function of E is a distorted triangle as in Figure VII-4b. The shapes of the sides of this triangle depend on the exact shape of the magnetic acceptance curve in Figure VII-1. E_l and E_u are taken to be the same as in Case I, even though the energy interval is much less well defined than in Case I.

Case III, $T < r_b - r_a$

Again, particles are just detected at $E = E(r_a)$. However, now as soon as E reaches $E(T + r_a)$, the entire thickness (T) of the scatterer contributes, and continues to do so until $E = E(r_b)$. The thickness contributing then decreases as E increases further, becoming zero at $E = (T + r_b)$. A plot of Δt vs E for this case is given in Figure VII-4c.

For this case E_l and E_u are chosen as follows:

$$E_l = \frac{E(\Lambda_a) + E(T+\Lambda_a)}{2}$$

$$E_u = \frac{E(\Lambda_b) + E(T+\Lambda_b)}{2}$$

Notice the E_l no longer equals E_m, but approaches $E_m - \frac{\Delta E_m}{2}$ as $\frac{T}{\Lambda_b - \Lambda_a}$ approaches zero.

In the case of the carbon scatterer, Case I applies up to about 50 Mev for protons or 70 Mev for deuterons, and Case III applies above 70 Mev for protons, or 90 Mev for deuterons. In the case of the Cu and Pb scatterers, Case I applies throughout the entire interval. Figure VII-5 gives the values of E_l and E_u as a function of E_m for copper and lead, E_l in these cases being equal to E_m throughout the whole range.

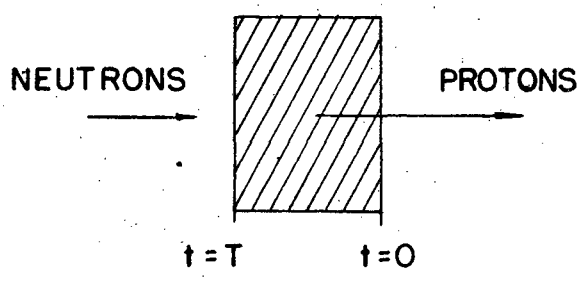

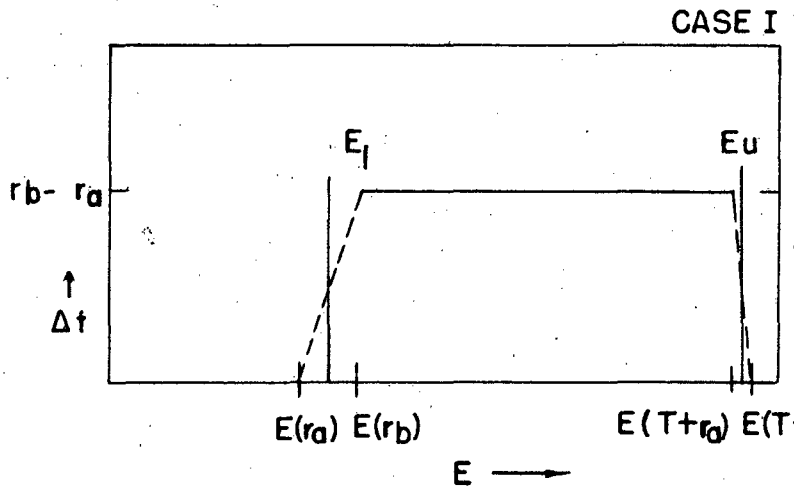

FIG VII - 4a

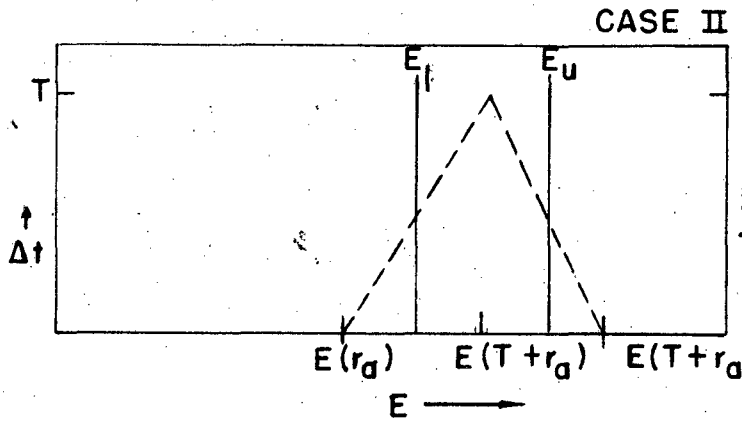

FIG VII - 4b

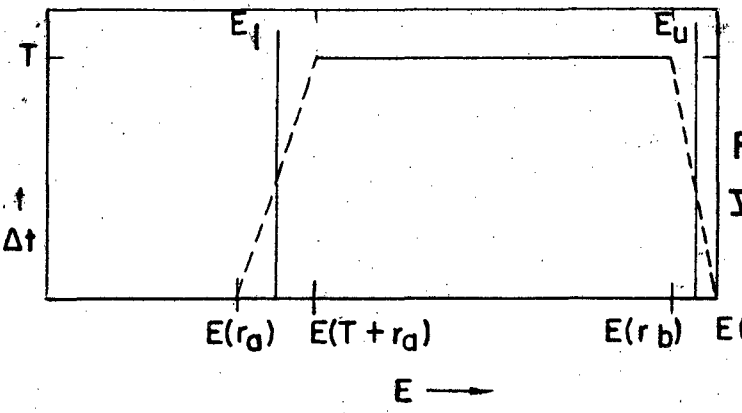

FIG VII - 4c

E. Example: Calculation of Relative Proton Spectrum at 0° from Data in Section V-C.

Table II gives the data and calculations in tabular form. Column I gives the magnetic field (in kilogauss) at which each measurement was made. Column II gives the corresponding E_m. Column III gives the proton count obtained (scatterer minus background). Column IV gives the monitor count. Column V gives the ratio of proton to minitor count, multiplied by 100 for convenience. Column VI gives the value of y, taken from Figure VII-3. Column VII gives $\overline{\Delta E(T)}$, which is equal to .12yE_m. Column VIII gives the relative $d\sigma_p$, which is the quotient of Column V divided by Column VII. Column IX gives the values of E_ℓ and E_u, between which the value of $d\sigma_p$ holds. Column X gives the probable error based on statistical considerations only.

TABLE II

I Kilo-gauss	II R_m	III Proton Count	IV Monitor Count	V $\frac{(III)}{(IV)} \times 100$	VI y	VII $\Delta E(T)$	VIII $d\sigma_p$	IX $E_x - E_a$	X Error
4.47	23	31	175	17.7	.87	2.4	7.4	23-31	1.2
5.20	31	31	123	25.2	.92	3.4	7.4	31-38	1.2
5.75	38	27	86	31.4	.94	4.3	7.3	38-44	1.2
6.35	46	47	127	37.0	.96	5.4	6.9	56-51	1.1
7.40	63	78	137	57.0	.98	7.4	7.7	63-68	0.9
8.05	74	35	116	30.2	.98	8.7	3.5	72-80	0.6
8.90	93	21	137	15.3	.99	11.0	1.4	90-97	0.3
9.60	108	3	105	3.0	.99	12.8	0.2	104-112	0.1

VIII. DETERMINATION OF ABSOLUTE CROSS SECTIONS

A. Principles of Determination

Table II in Section VII gives the relative differential cross sections at various energies for the production of knock out protons at an angle of 0^{o}. A similar table may also be prepared for the deuterons and tritons. Let us assume that the values in the table are equal to the absolute differential cross section, in units of millibarns per steradian per Mev, multiplied by some factor K. If we now make a plot of these cross sections vs energy for all three types of particles, and numerically integrate under each curve between some lower energy limit such that the ranges of all three types are identical (i.e., three different lower limits) and infinity, we obtain the total cross section, again multiplied by this same K, for producing secondary particles which have a range greater than some predetermined value. By comparing this latter cross section with a known absolute n-p differential cross section, we may eliminate K and put all of the various differential cross sections on an absolute scale.

B. Apparatus

The experimental set up used to make this comparison is shown in Figure VIII-1. It is identical with the apparatus used in the n-p scattering experiments of Hadley, et al. The counter telescope is essentially the same as that shown in Figure IV-3 except that the first tube shown in the Figure is replaced by a tube identical to the second, since here the counters are used merely as proton detectors. The location of the experi-

mental set up and the collimating system are the same as in the case of the experiments done with the magnet.

The scatterers are 1" by 2" pieces of carbon (480 mg/cm^2), copper (713 mg/cm^2), lead (910 $\frac{mg}{cm^2}$), and polyethylene (420 mg/cm^2). These thicknesses were chosen so that each of the targets would have the same integrated stopping power, that is, a high energy particle would lose the same amount of energy in passing through each one.

The monitor was a bismuth fission chamber, which is sensitive only to high energy neutrons.

C. Procedure

The apparatus is set up in the same way as in the n-p scattering experiments, with the angle θ equal to 25°. The polyethylene, (C_nH_{2n}), target is put in place, and an absorber is placed between the second and third tubes. The thickness of the absorber is such that a proton originating in the center of scatterer with an energy of 54 Mev (= 66 cos^2 25 Mev) can just penetrate to the third counter. This lower energy limit is the same as that used in the n-p scattering experiments; it allows only those neutrons with energies greater than 66 Mev to produce detectable recoil protons from the H in the C_nH_{2n}.

With this arrangement, the ratio of proton counts to monitor counts is determined. This process is repeated with the carbon scatterer in place, and with no scatterer. From these three measurements we can determine in an obvious way the number of protons per minitor count which

originated in n-H interactions. Let us denote this number by N_H.

The absorber is now removed, and runs are made successively with the carbon, copper, and lead scatterers and with no scatterer. The total absorbing material in the system, including one-half of the thickness of the scatterer, is in this case equivalent to 460 mg/cm^2 of carbon. The energy of a proton just able to penetrate this is 20 Mev, and the corresponding energies for deuterons and tritons are 27 and 33 Mev, respectively. Let us call the ratio of scatterer count to monitor count (with the blank count subtracted) N_C, N_{Cu} and N_{Pb}, respectively.

D. Analysis of Data

The quantity N_H, defined above, is related to the neutron flux as follows:

$$N_H = \Omega \, \sigma_{np}(25^\circ) \, n_H \, \eta_n$$

where Ω = solid angle subtended by the counter telescope as seen from the scatterer.

σ_{np} = the differential n-p cross section per unit solid angle for scattering protons at the laboratory angle $\theta = 25^\circ$.

n_H = the number of hydrogen atoms in that part of the scatterer which is exposed to the neutron beam.

η_n = the flux density of neutrons with energies greater than 66 Mev. The flux density in this case is expressed in units of neutrons per cm^2 per monitor count. A similar relation holds for N_C and the others:

$$N_c = \Omega \left(\sigma_{p>20}(25^\circ) + \sigma_{d>27}(25^\circ) + \sigma_{t>33}(25^\circ) \right) n_c \, \eta_n'$$

where $\sigma_{p>20}(25^\circ)$ is the differential cross section for carbon for producing secondary protons with energies greater than 20 Mev, and $\sigma_{d>27}(25^\circ)$ and $\sigma_{t>33}(25^\circ)$ are defined similarly. We shall use the symbol $\Sigma(25^\circ)$ to denote the sum of these cross sections.

n_c = the number of carbon atoms in that part of the scatterer exposed to the neutron beam.

n_n' = the flux density, in units of number per cm^2 per monitor count, of the neutrons which produce the observed particles.

Combining these two relations we have

$$\Sigma(25^\circ) = \frac{N_c}{N_H} \frac{n_H}{n_c} \frac{n_n}{n_n'} \sigma_{np}(25^\circ)$$

Of the quantities of the right, $\frac{N_c}{N_H}$ is observed in this experiment, $\frac{n_H}{n_c}$ is determined by obvious mechanical measurements, and $\sigma_{np}(25^\circ)$ is known from the n-p scattering experiments. $\frac{n_n}{n_n'}$ would be unity if the neutron beam contained no neutrons with energies less than 66 Mev, or if neutrons below 66 Mev produced no secondary particles. The spectrum of the neutron beam shown in Figure IV-1 gives an idea of the total number of neutrons with energies below 66 Mev. However, because the reactions $C^{12}(n,D)B^{11}$, $C^{12}(n,P)B^{12}$, and $C^{12}(n,T)B^{10}$ are highly endothermic, not all of the neutrons below 66 Mev are effective. For instance, only those neutrons above 37 Mev can produce detectable protons, and only neutrons above 45 Mev can produce detectable deuterons. Furthermore, the probability of a reaction of this type is very small immediately above its threshhold, so that we may say,

roughly speaking, that n_n' includes all those neutrons with energies above about 50 Mev. Using this energy as an effective lower limit for the flux involved in n_n', we find by numerical integration of the appropriate parts of Figure IV-1, that n_n/n_n' is probably not smaller than 0.9. This ratio could, of course, be practically unity, and in the calculation of Σ we shall take it to be one.

Using the value of $\sigma_{np}(25°) = .025$ barns found by Hadley et al, we obtain for the Σ's

$$\Sigma_C(25°) = .058 \text{ barns/steradian}$$
$$\Sigma_{Cu}(25°) = .112 \quad "$$
$$\Sigma_{Pb}(25°) = .140 \quad "$$

where Σ is the sum of the differential cross sections for producing protons with more than 20 Mev, deuterons with more than 27 Mev and tritons with more than 33 Mev, by bombardment with 90 Mev neutrons.

By simply changing the angle θ and measuring N_C, N_{Cu} and N_{Pb} at various other angles, the variation of Σ with θ can be found. Figure VIII-2 is a plot of the results obtained. It gives the values of the various Σ's for various θ's ranging from 6° to 135°.

Another way of describing the analysis in this section is to say that, by means of the measurements made with polyethylene scatterer, we have calibrated the monitor count in terms of the neutron flux, and then knowing the flux, we have measured the Σ's.

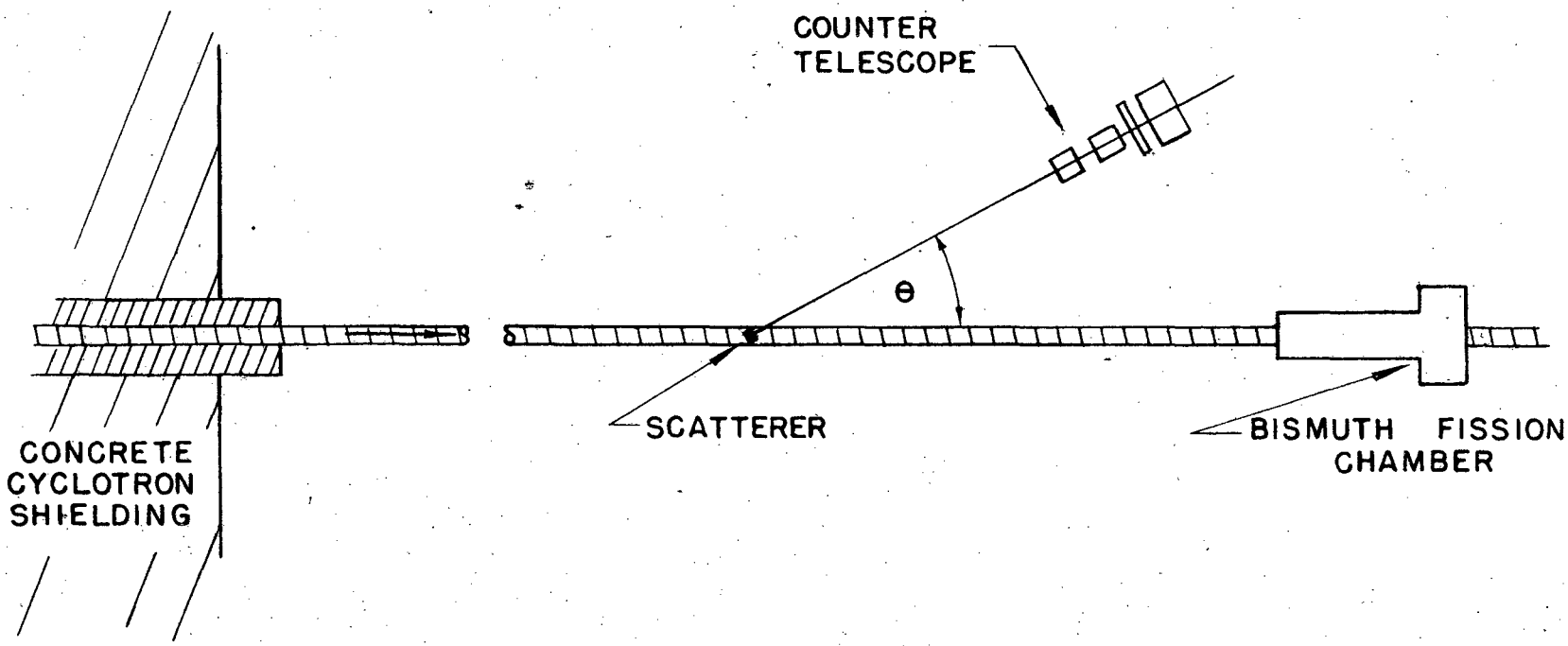
COUNTER
TELESCOPE
θ
SCATTERER
BISMUTH FISSION
CHAMBER
CONCRETE
CYCLOTRON
SHIELDING

FIG VIII -1

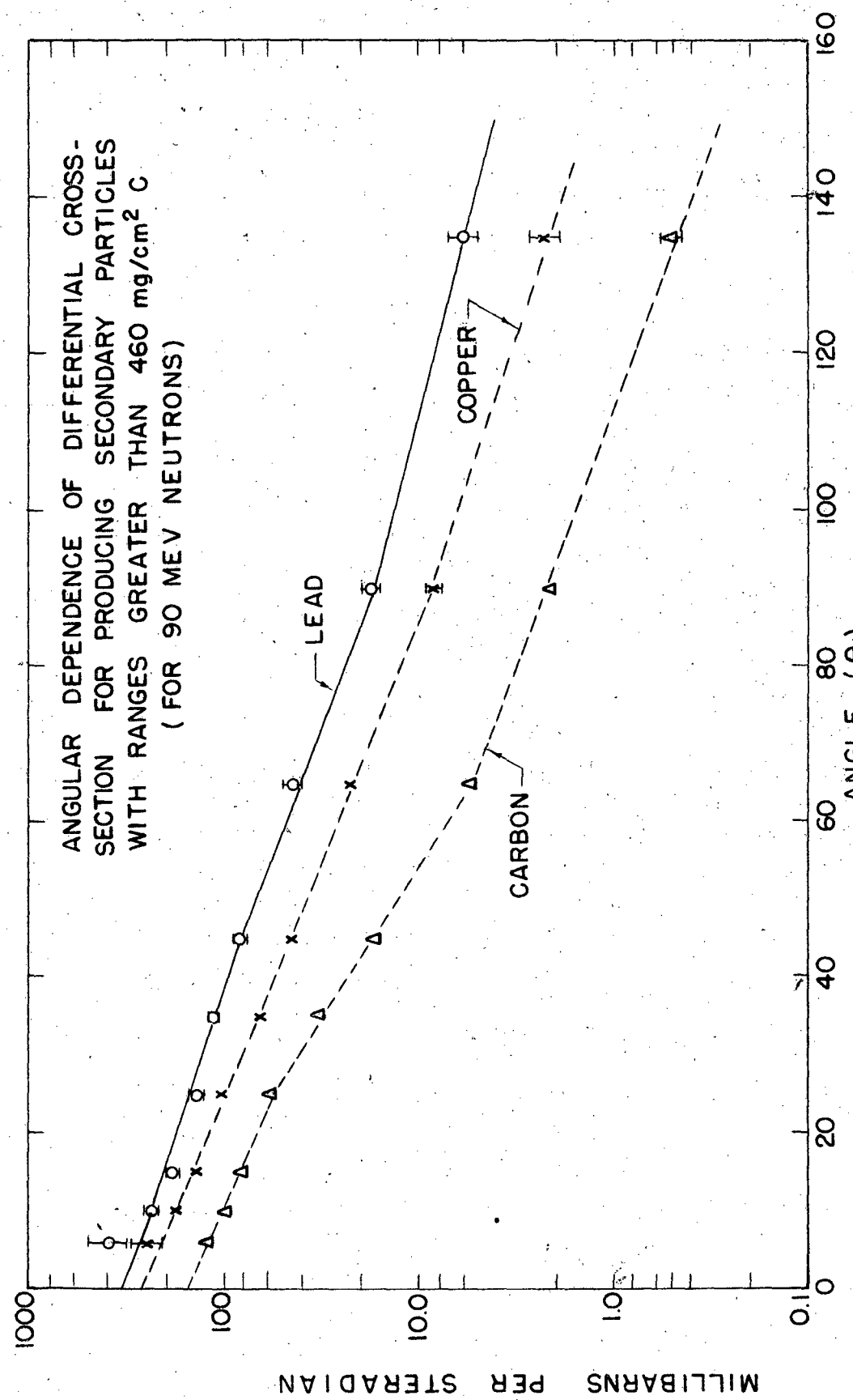
ANGULAR DEPENDENCE OF DIFFERENTIAL CROSS-SECTION FOR PRODUCING SECONDARY PARTICLES WITH RANGES GREATER THAN 460 mg/cm² C
(FOR 90 MEV NEUTRONS)
LEAD
COPPER
CARBON
MILLIBARNS PER STERADIAN
1000
100
10.0
1.0
0.1
0
20
40
60
80
100
120
140
160
ANGLE (θ)

FIG. VIII -2

IX. FINAL RESULTS

A. Form of Presentation

Data of the form described in Section V were obtained using C, Cu and Pb targets at $\theta = 0^\circ$, 12°, 25° and 45°. These data were analyzed using the methods described in Section VII to find the relative differential cross sections as a function of energy at each angle, and then were further treated as described in Section VIII to find the absolute values of these differential cross sections.

The final results are presented in tabular form in Tables III-V, and in graphical form in Figures IX-1 to IX-6. In the tables the following items are recorded: the angle at which the measurements were made, the type of particle, the energy range in which the given cross section applies, the differential cross section in units of millibarns ($10^{-27}cm^2$) per steradian per Mev, and the probable error of the measurement.

In the case of carbon, the proton and deuteron curves are plotted using each of the tabulated cross sections in Table III. However, the triton cross sections listed there are not plotted individually, but only the average of these values over a wide energy range is shown. The reason for plotting the triton data in this way is that the range of energies to which each value of $d\sigma_c$ applies is so large, and so overlaps the neighboring values, that no spectral details could be seen.

In the case of copper and lead the proton results are treated in the same way as in the case of carbon, and the deuteron results are treated in

TABLE III

PARTICLES FROM CARBON

$\frac{d\sigma}{d\Omega dE}$ (millibarns / steradian Mev)

Protons 0° Energy	$d\sigma_p$	Deuterons 0° Energy	$d\sigma_d$	Protons 12° Energy	$d\sigma_p$	Deuterons 12° Energy	$d\sigma_d$
23-31	1.53 ± .20	29-39	.54 ± .12	20-30	1.32 ± .12	26-39	.42 ± .08
31-38	1.53 ± .20	31-43	.60 ± .10	28-35	1.09 ± .10	30-41	.38 ± .06
38-44	1.50 ± .20	37-47	.53 ± .10	37-43	1.14 ± .08	35-45	.50 ± .06
46-51	1.43 ± .15	46-55	.70 ± .10	45-50	1.01 ± .08	39-49	.59 ± .06
63-68	1.59 ± .15	54-65	1.41 ± .15	50-56	1.15 ± .08	45-52	.54 ± .06
72-80	.70 ± .12	60-69	1.44 ± .10	50-63	1.05 ± .08	55-62	.65 ± .06
90-97	.27 ± .05	67-74	1.07 ± .10	67-72	.80 ± .06	65-70	.61 ± .06
99-107	.05 ± .02	71-78	.77 ± .10	73-80	.48 ± .04	73-79	.27 ± .04
		78-85	.27 ± .05	97-96	.25 ± .04	85-92	.08 ± .02
		87-94	.29 ± .05	105-115	.06 ± .03		

25° Energy	$d\sigma_p$	Energy	$d\sigma_d$	45° Energy	$d\sigma_p$	Energy	$d\sigma_d$
19-28	.82 ± .06	27-40	.22 ± .04	17-27	.47 ± .05	25-38	.09 ± .02
27-34	.93 ± .05	32-43	.31 ± .04	24-32	.47 ± .05	32-43	.08 ± .02
39-44	.85 ± .05	39-49	.32 ± .03	30-37	.32 ± .03	39-49	.06 ± .01
53-58	.61 ± .03	45-54	.14 ± .03	40-45	.18 ± .03	44-53	.07 ± .01
65-70	.47 ± .03	57-65	.20 ± .03	51-56	.17 ± .02	63-69	.02 ± .01
87-94	.15 ± .03	80-89	.07 ± .02	75-82	.07 ± .01		
				84-92	.07 ± .01		

Carbon 0° Tritons:
35-70 $d\sigma_t$ = .17

TABLE IV
PARTICLES FROM COPPER

$\frac{d\sigma}{d\Omega dE}$ $\left(\frac{\text{millibarns}}{\text{steradian Mev}}\right)$

0°

Protons		Deuterons		
Energy	$d\sigma_p$	Energy	$d\sigma_d$	
23-48	3.1±.3	31-69	1.0	
31-54	3.4 ±.3	37-72	1.4	
38-61	2.7±.3	47-79	.75	
46-67	2.8±.3	54-84	.9	.9±.1
63-78	1.9±.2	60-88	.9	
74-88	1.4±.2	67-93	.8	
93-100	.2±.1	71-96	.45±.1	
		78-102	.2 ±.1	

12°

Protons		Deuterons		
Energy	$d\sigma_p$	Energy	$d\sigma_d$	
20-47	2.2±.2	26-67	.22	
28-53	1.7±.2	30-69	.78	
37-60	1.4±.2	35-71	.74	
45-65	2.0±.2	40-74	.37	.56±.06
50-69	1.8±.15	47-79	.55	
58-75	1.9±.15	57-85	.63	
67-83	1.2±.1	67-93	.59	
77-92	.6±.1	77-100	.30±.1	
91-102	.5±.1	89-110	.15±.05	
100-110	.06±.02			

25°

Energy	$d\sigma_p$	Energy	$d\sigma_d$	
19-47	1.63±.1	27-67	.29	
27-53	1.67±.1	32-69	.43	
39-61	1.44±.1	39-73	.33	.34±.04
53-72	1.02±.07	45-77	.32	
65-82	.70±.05	57-86	.14	
78-93	.27±.05	69-93	.15	
90-104	.13±.15			

45°

Energy	$d\sigma_p$	Energy	$d\sigma_d$	
24-51	.94±.1	25-67	.17	
30-58	.74±.06	32-69	.10	
40-62	.48±.04	39-73	.09	.11±.02
51-70	.34±.02	45-77	.09	
63-80	.24±.02	53-83	.06-.02	
77-92	.15±.01	63-90	.04-.02	
87-101	.06±.01			

TABLE V
PARTICLES FROM LEAD

$\frac{d\sigma}{d\Omega dE}$ $\left(\frac{\text{millibarns}}{\text{steradian Mev}}\right)$

0°

Protons Energy	$d\sigma_p$	Deuterons Energy	$d\sigma_d$	
23-49	4.3±.8	31-65	0	
31-53	4.8±.7	37-68	1.1	
38-58	2.6±.5	47-75	2.2	1.5±.25
46-64	3.7±.5	54-81	2.3	
69-78	1.9±.3	60-86	1.9	
74-88	2.3±.3	67-92	1.0±.3	
93-100	0.4±.2	71-95	1.2±.3	
		78-100	.9±.3	

12°

Protons Energy	$d\sigma_p$	Deuterons Energy	$d\sigma_d$	
20-47	1.6±.25	26-63	.25	
28-52	2.0±.25	30-64	.45	
37-59	2.7±.2	35-67	.70	
45-64	2.2±.2	40-70	.25	.65±.1
50-69	2.0±.2	47-77	.90	
58-74	1.7±.2	57-84	.90	
67-83	1.4±.2	67-92	.60	
77-92	.6±.1	77-100	.35	
91-102	.6±.1	89-110	0	
100-110				

25°

Energy	$d\sigma_p$	Energy	$d\sigma_d$	
19-46	1.7±.2	27-63	.36	
27-51	1.9±.1	32-65	.36	
39-60	1.6±.1	39-69	.36	
59-70	1.0±.1	45-74	.20	.31±.05
65-80	.68±.06	57-84	.10	
78-91	.15±.03	67-92	.10	
90-103	.10±.03			

45°

Energy	$d\sigma_p$	Energy	$d\sigma_d$	
24-49	1.2±.15	25-62	.24	
30-53	.83±.10	32-65	.25	
40-60	.74±.07	39-70	.15	
51-69	.55±.03	44-74	.10	.19±.02
63-78	.28±.03	53-80	.035	
77-91	.23±.03			
83-96	.06±.01			

the same way as in the case of the tritons from carbon, for the same reason as in that case.

No counts were obtained which could with any certain be attributed to tritons, except for the case of the zero degree carbon observations. In that case they contributed four percent of the total cross section and their yield in all other cases is probably less than one percent.

B. Discussion of Error

The tabulated probable errors include only the expected statistical fluctuations in the relative values of the cross sections, and do not include the additional errors which can arise in the determination of the absolute scale. This latter error is probably of the order of $\pm$ 25%, and includes, besides the usual statistical factors, which are, in fact, quite small, a number of other factors. Of these the principal ones are the uncertainty of the absolute value of the differential n-p cross section involved in the calculation of the absolute cross sections, and the uncertainty involved in the numerical integration of the plots of the relative differential cross sections.

The case of the data at 0° deserves special mention in regard to these errors, for at that angle the absolute cross section for producing the secondaries was not measured at all. It can be seen in Figure VIII-2 that the cross sections at those points where they were measured (6°,10°, 15°,25°, etc.) fall quite well on a pure exponential curve. This curve was extrapolated to zero, and the extrapolated value was used in normalizing the zero degree relative cross sections. This extrapolation is not too dangerous, since, as will be seen later, the physics of the situation indicates that there should be no marked singularities in the forward direc-

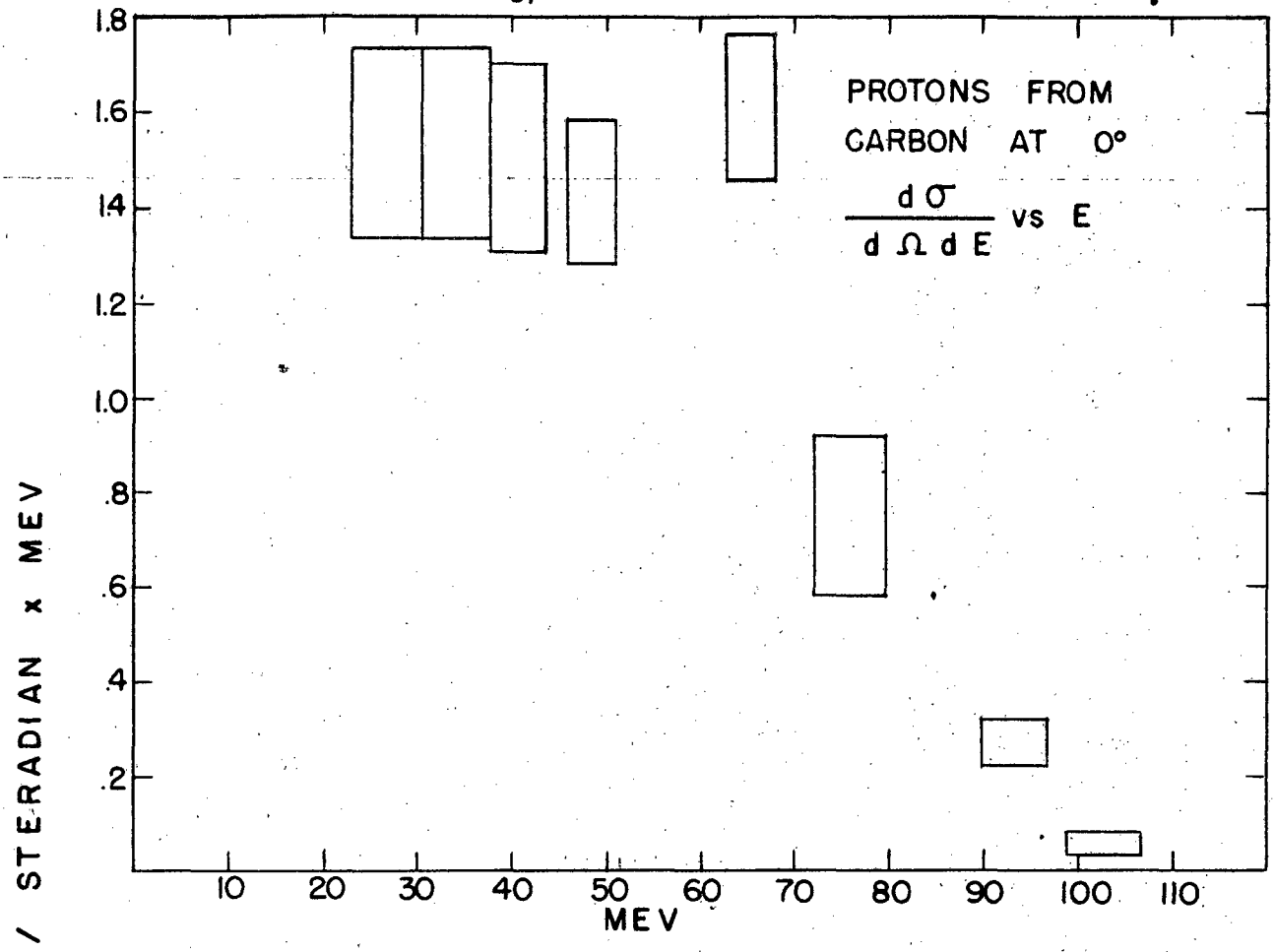
PROTONS FROM
CARBON AT 0°
dσ / dΩ dE vs E
MILLIBARNS / STERADIAN x MEV
1.8
1.6
1.4
1.2
1.0
.8
.6
.4
.2
10 20 30 40 50 60 70 80 90 100 110
MEV

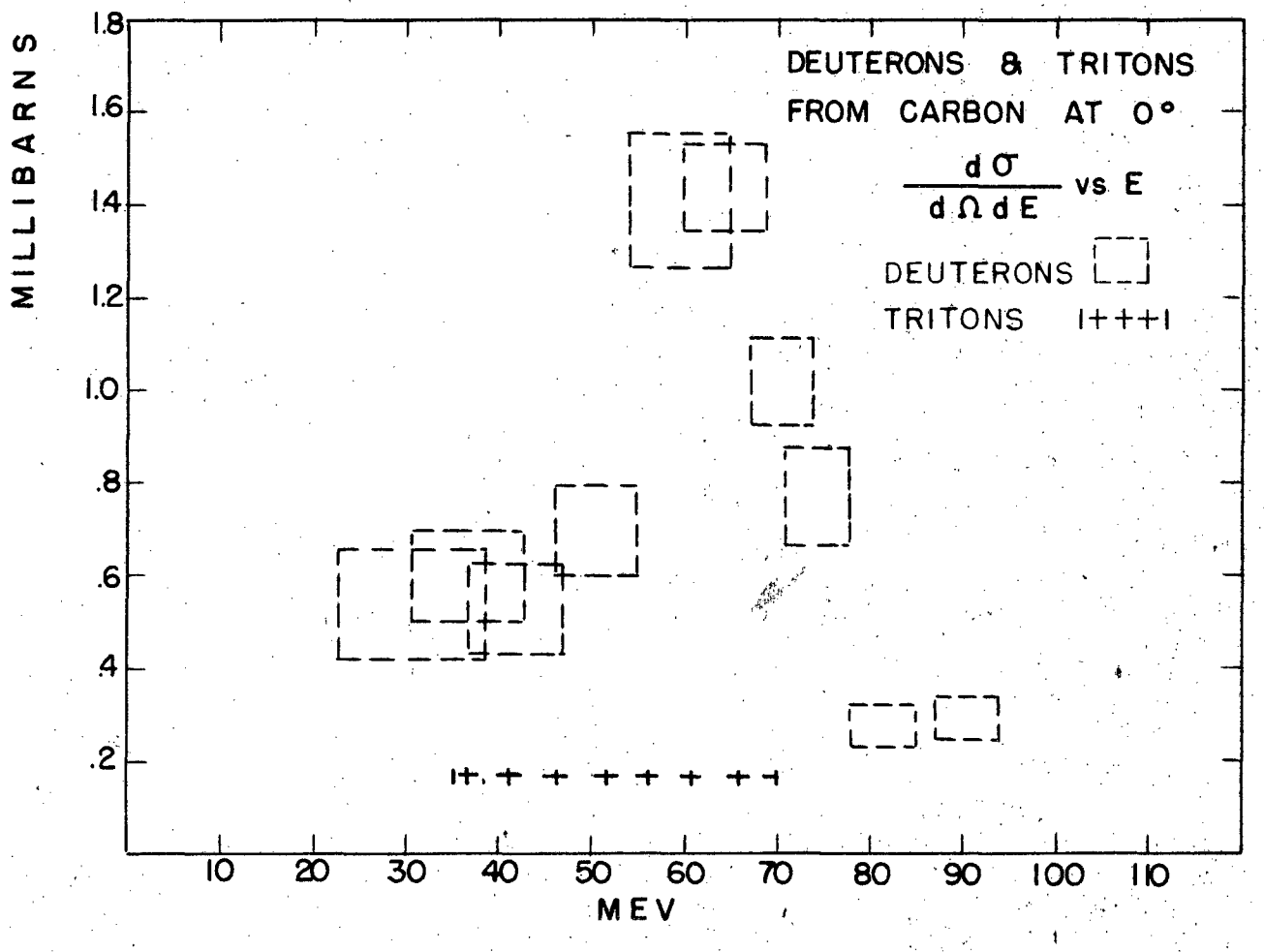
DEUTERONS & TRITONS
FROM CARBON AT 0°
dσ / dΩ dE vs E
DEUTERONS
TRITONS
1.8
1.6
1.4
1.2
1.0
.8
.6
.4
.2
10 20 30 40 50 60 70 80 90 100 110
MEV

FIG IX-1

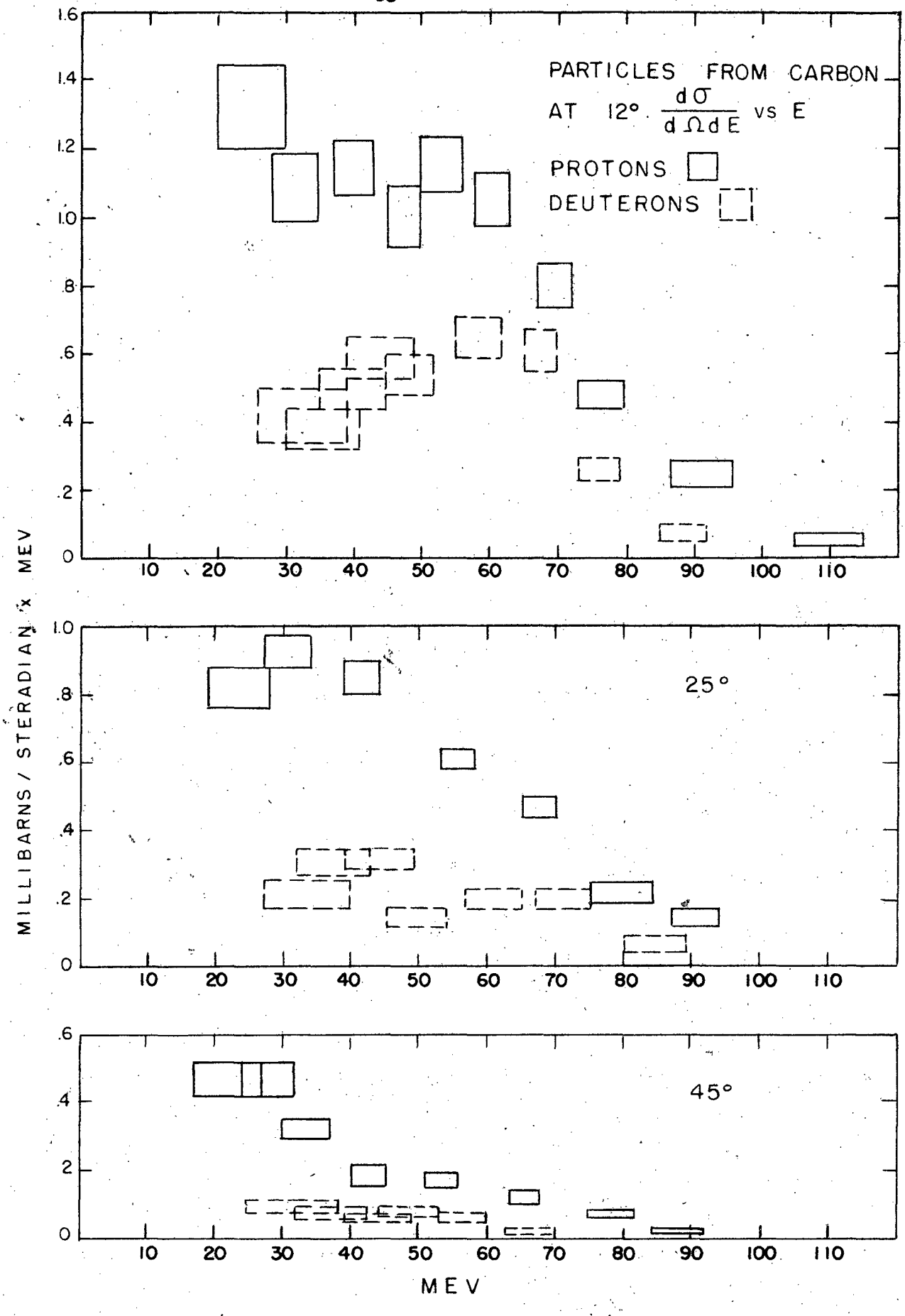
PARTICLES FROM CARBON
AT 12°. dσ/dΩdE vs E
PROTONS
DEUTERONS
25°
45°
MILLIBARNS / STERADIAN x MEV
MEV

FIG IX - 2

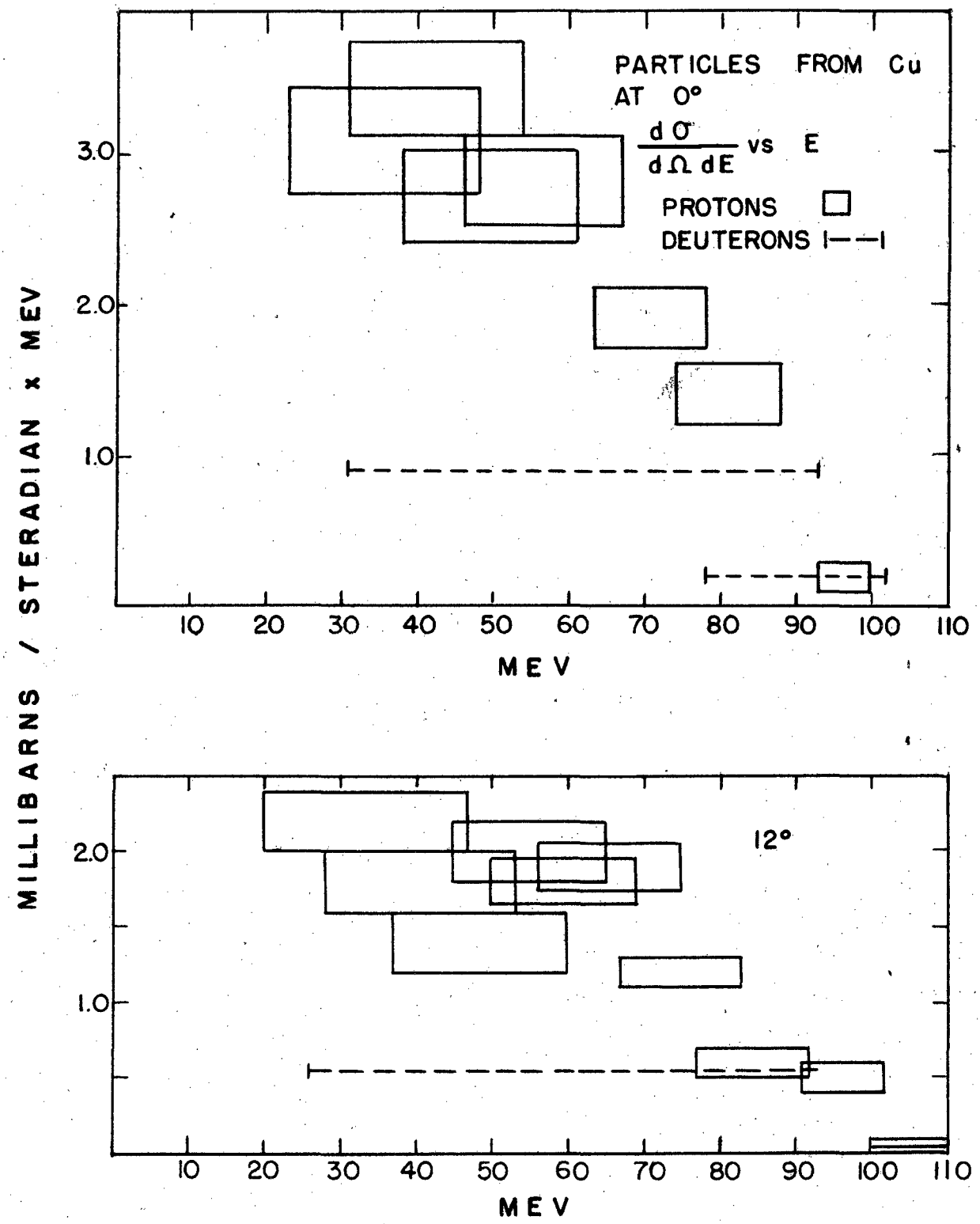
PARTICLES FROM Cu
AT 0°
dσ/dΩ dE vs E
PROTONS
DEUTERONS
3.0
2.0
1.0
10 20 30 40 50 60 70 80 90 100 110
MEV
12°
2.0
1.0
10 20 30 40 50 60 70 80 90 100 110
MEV
MILLIBARNS / STERADIAN x MEV

FIG. IX - 3

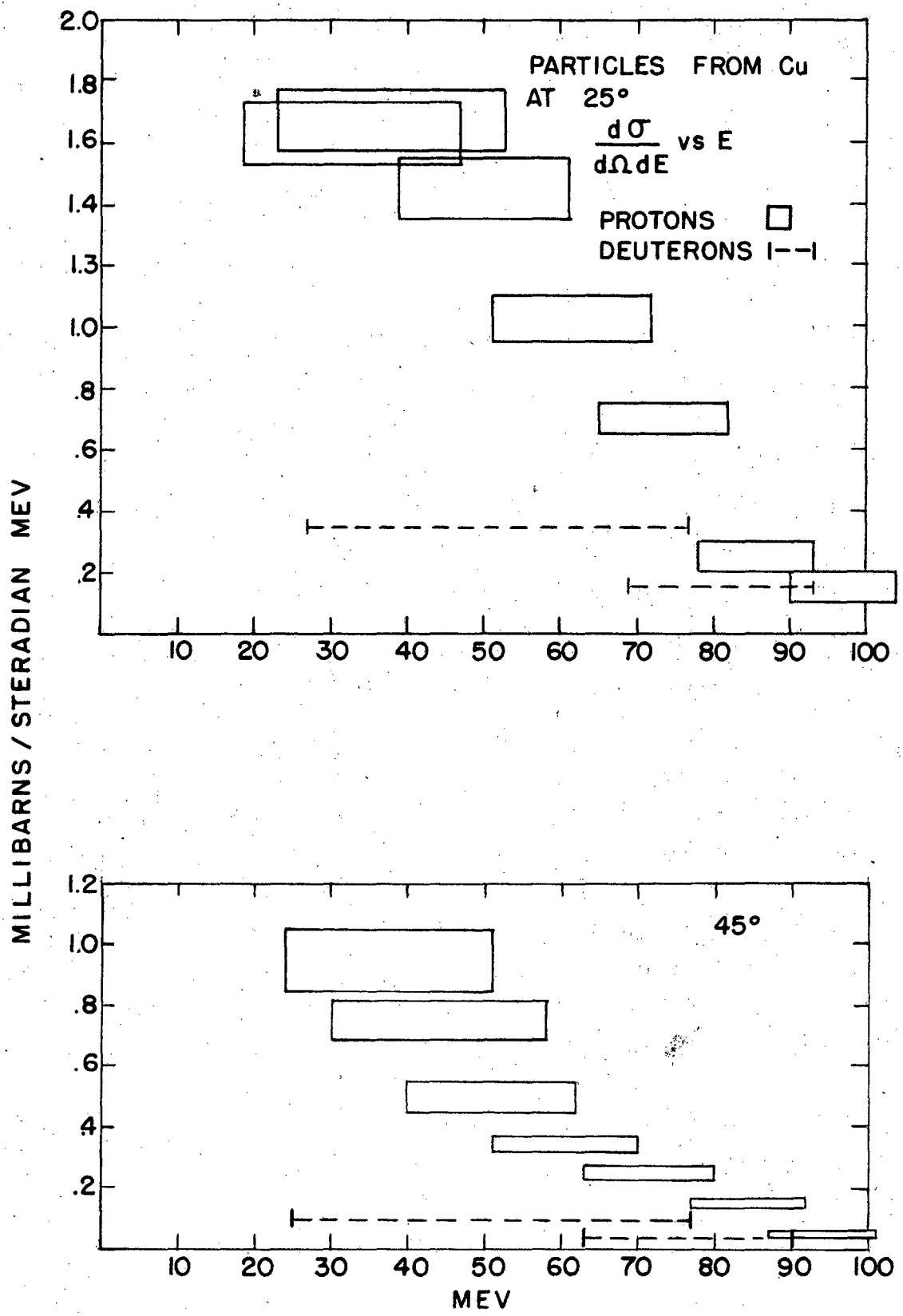
PARTICLES FROM Cu
AT 25°
dσ/dΩdE vs E
PROTONS
DEUTERONS
45°
MILLIBARNS / STERADIAN MEV
MEV
2.0
1.8
1.6
1.4
1.3
1.0
.8
.6
.4
.2
1.2
10
20
30
40
50
60
70
80
90
100

FIG IX-4

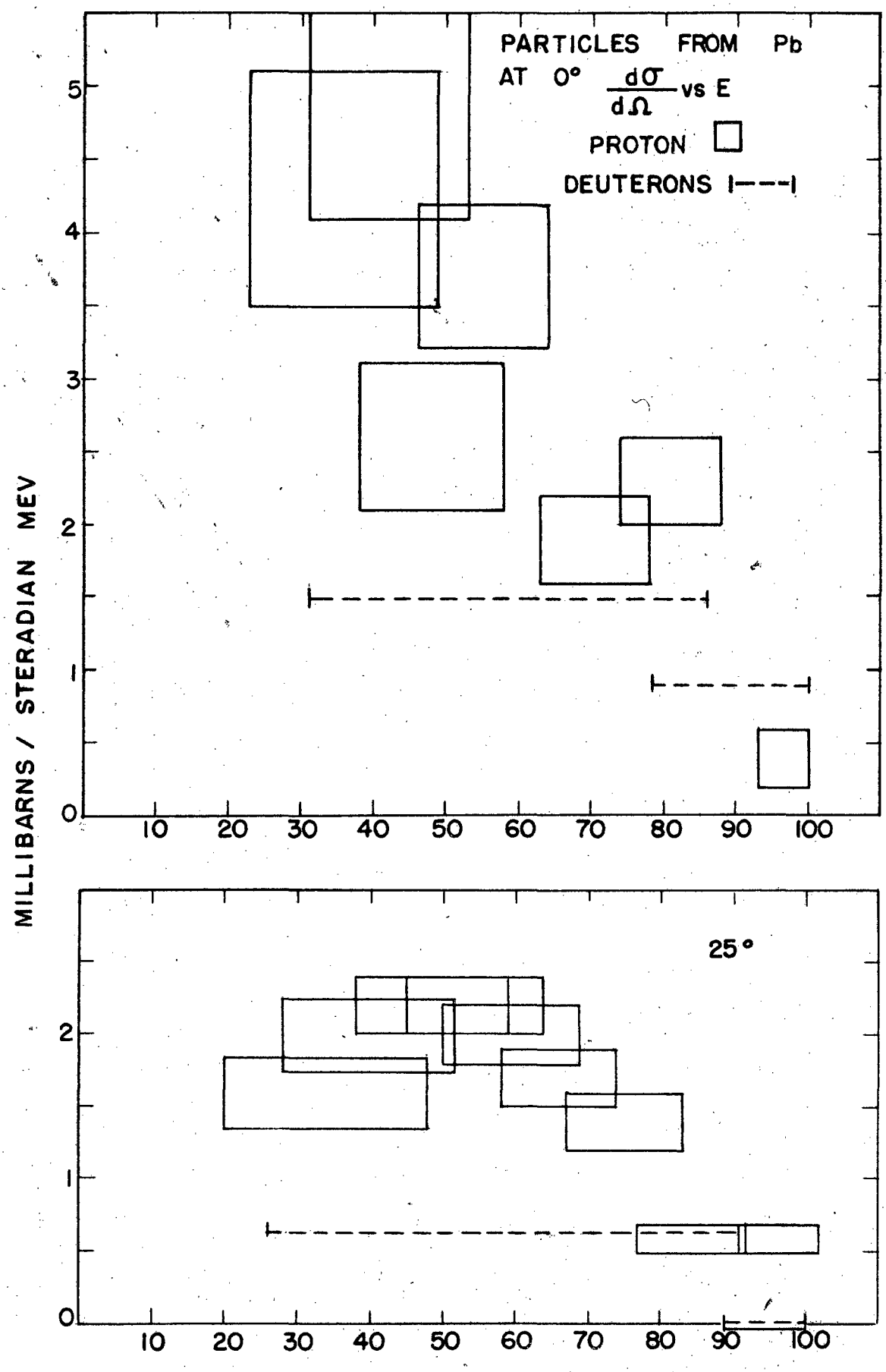
PARTICLES FROM Pb
AT 0° dσ/dΩ vs E
PROTON
DEUTERONS
MILLIBARNS / STERADIAN MEV
0
1
2
3
4
5
10
20
30
40
50
60
70
80
90
100
25°

FIG IX - 5

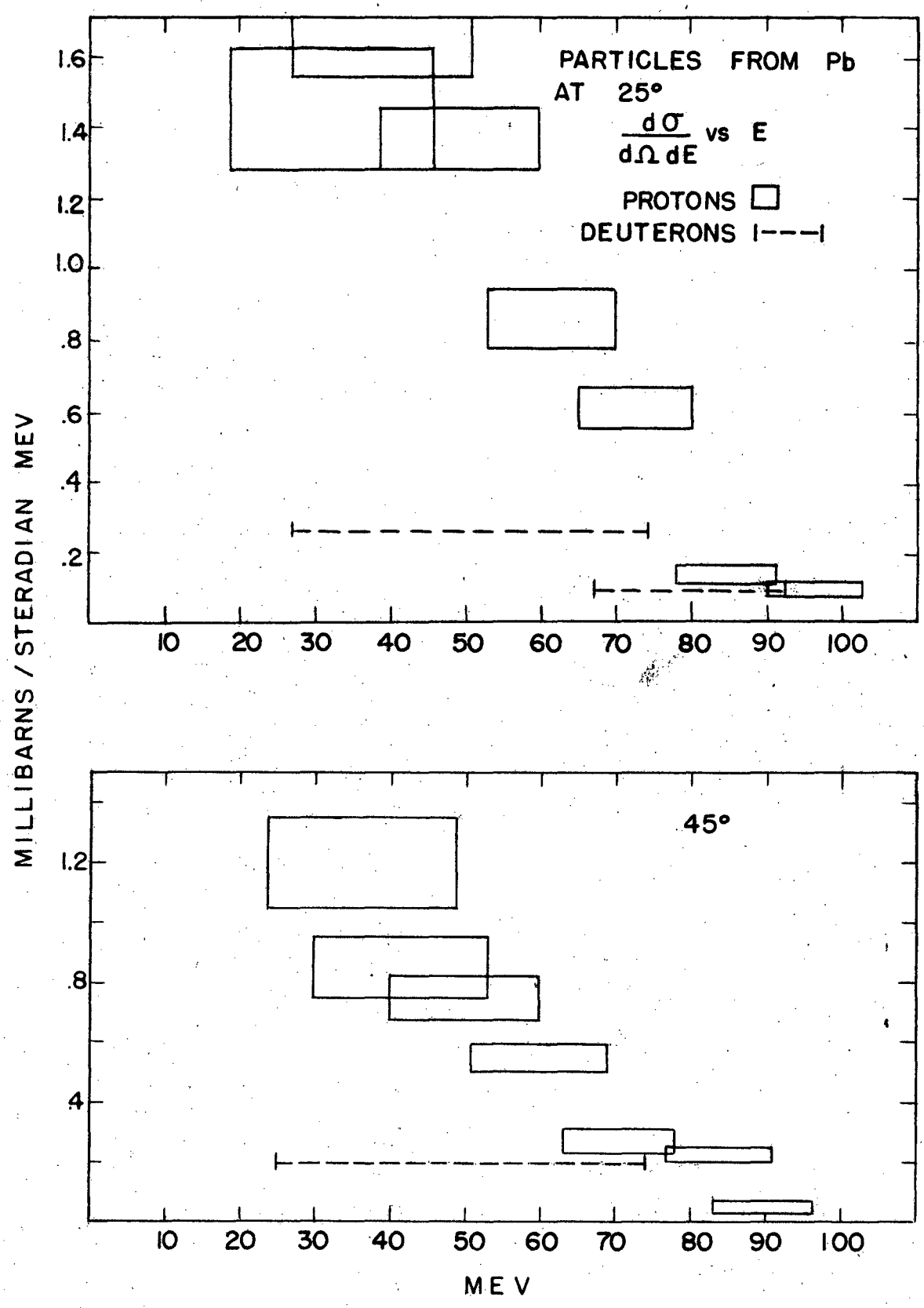
PARTICLES FROM Pb
AT 25°
dσ/dΩ dE vs E
PROTONS
DEUTERONS
45°
MILLIBARNS / STERADIAN MEV
MEV
1.6
1.4
1.2
1.0
.8
.6
.4
.2
10
20
30
40
50
60
70
80
90
100

FIG IX - 6

tion.

C. Total Cross Sections

In this section we shall attempt to estimate the total cross sections of the various processes of interest, and discuss the validity of these calculations.

The total cross section of a carbon nucleus for producing protons having energies greater than E_0 when bombarded by 90 Mev neutrons is

$$\sigma_{p>E_0}(C) = 2\pi \int_{E_0}^{\infty} \int_{0}^{\pi} \frac{d\sigma_p(\theta,E)}{dE\, d\Omega}\, dE\, d(\cos\theta)$$

Since $\frac{d\sigma(\theta,E)}{dE\,d\Omega}$ has been determined at only four angles, (0^0, 12^0, 25^0, and 45^0), the calculation of $\sigma_{p>E_0}(C)$ is feasible only if two conditions are satisfied, namely, if most of the particles lie within the angular range of 0^0 - 45^0, and if we have some way of reasonably estimating the value of $d\sigma_p$ at angles between those at which measurements were made. In order to investigate the question of whether or not these two conditions hold, let us consider the plots of $\Sigma(\theta)$ given in Figures VIII-2.

$\Sigma(\theta)$ is the differential cross section, in millibarns per steradian, for producing all particles with ranges greater than 460 mg/cm^2 of carbon, and in terms of the definitions above:

$$2\pi \int_{0}^{\pi} \Sigma(\theta)\, d(\cos\theta) = \sigma_{d>27\,Mev} + \sigma_{p>20\,Mev}$$

As shown in the figure, the values of $\Sigma(\theta)$, when plotted on semi-log paper as a function of θ, fall very closely on a series of straight lines, each line extending over a considerable range of angles. Therefore, to find $\sigma_{d>27} + \sigma_{p>20}$ we have only to find the equations of these lines and to perform the

appropriate integrations. In the same way, we may find what fraction of the particles are emitted within 45° of the forward direction.

Table VI gives the results of these calculations.

Table VI

	$2\pi\int_0^{\pi}\Sigma(\theta)\,d\cos\theta$	$2\pi\int_0^{\pi/4}\Sigma(\theta)\,d\cos\theta$	fraction of particles in first 45°
C	117	87	.75
Cu	293	170	.58
Pb	499	276	.55

The table shows that for all elements, and especially for carbon, most of the particles lie in the region in which the detailed measurements were made. Furthermore, as will be shown shortly, the deuteron cross section drops off much faster with θ than $\Sigma(\theta)$, and so it is highly probably that a larger fraction of the deuterons lies within the range of the detailed measurements.

In order to show that the other conditions holds, let us consider Figures IX-7,8,9. In these figures the following differential cross sections are plotted:

$$\Sigma(\theta),\quad \frac{d\sigma^{(\theta)}_{p>20\,Mev}}{d\Omega},\quad \frac{d\sigma^{(\theta)}_{p>35\,Mev}}{d\Omega},\quad \frac{d\sigma^{(\theta)}_{d>27\,Mev}}{d\Omega}$$

where the $\Sigma(\theta)$ are taken from Figure VIII-2 and

$$\frac{d\sigma^{(\theta)}_{x>E_0}}{d\Omega} = \int_{E_0}^{\infty}\frac{d\sigma_x(\theta,E)}{d\Omega\,dE}\,dE$$

These latter cross sections are found by numerically integrating the appropriate curves in Figures IX-1 to IX-6. The $\Sigma(\theta)$ values, as mentioned

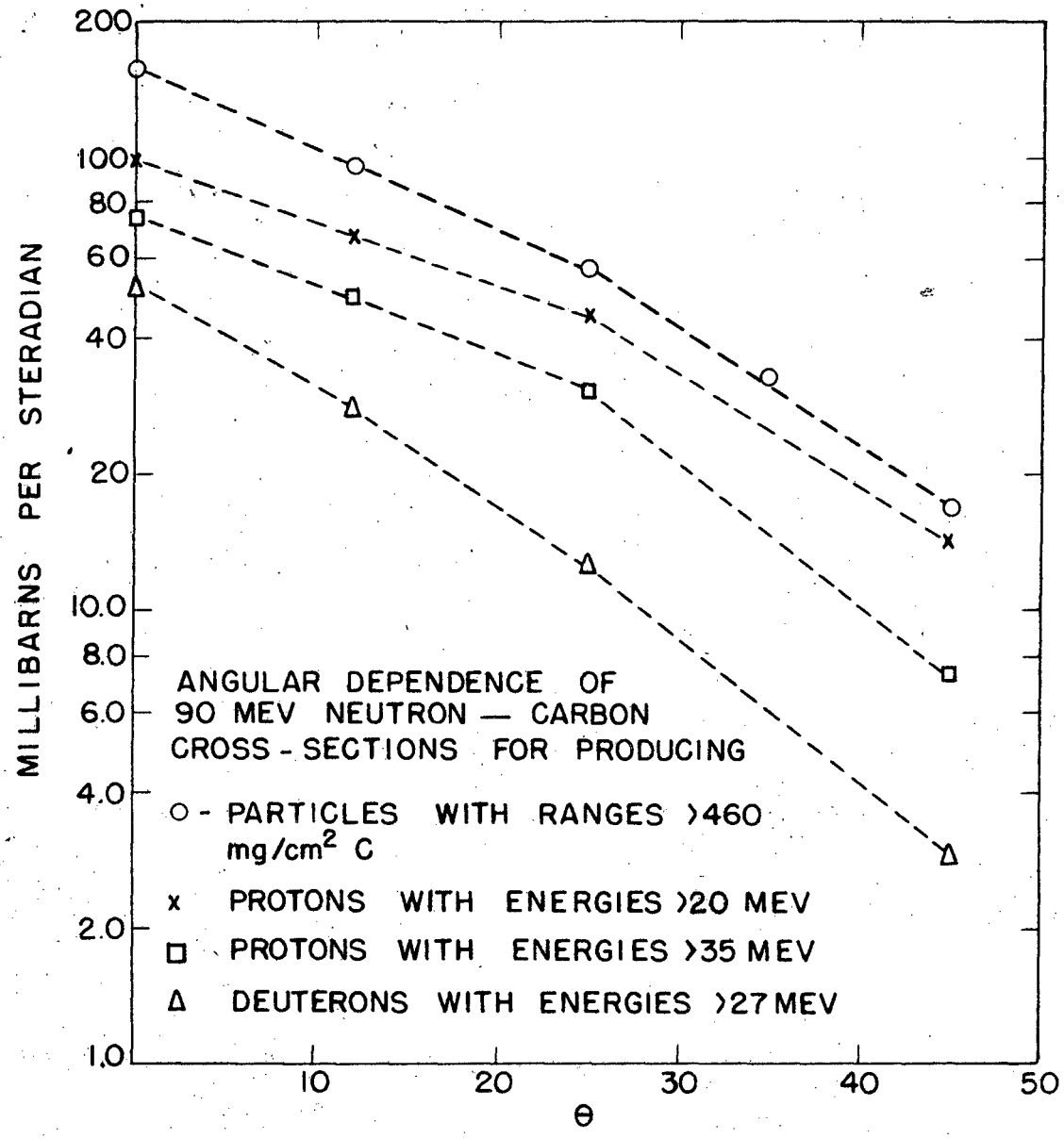
MILLIBARNS PER STERADIAN
200
100
80
60
40
20
10.0
8.0
6.0
4.0
2.0
1.0
10
20
30
40
50
θ
ANGULAR DEPENDENCE OF
90 MEV NEUTRON — CARBON
CROSS-SECTIONS FOR PRODUCING
○ - PARTICLES WITH RANGES >460 mg/cm² C
x PROTONS WITH ENERGIES >20 MEV
□ PROTONS WITH ENERGIES >35 MEV
Δ DEUTERONS WITH ENERGIES >27 MEV

FIG IX-7

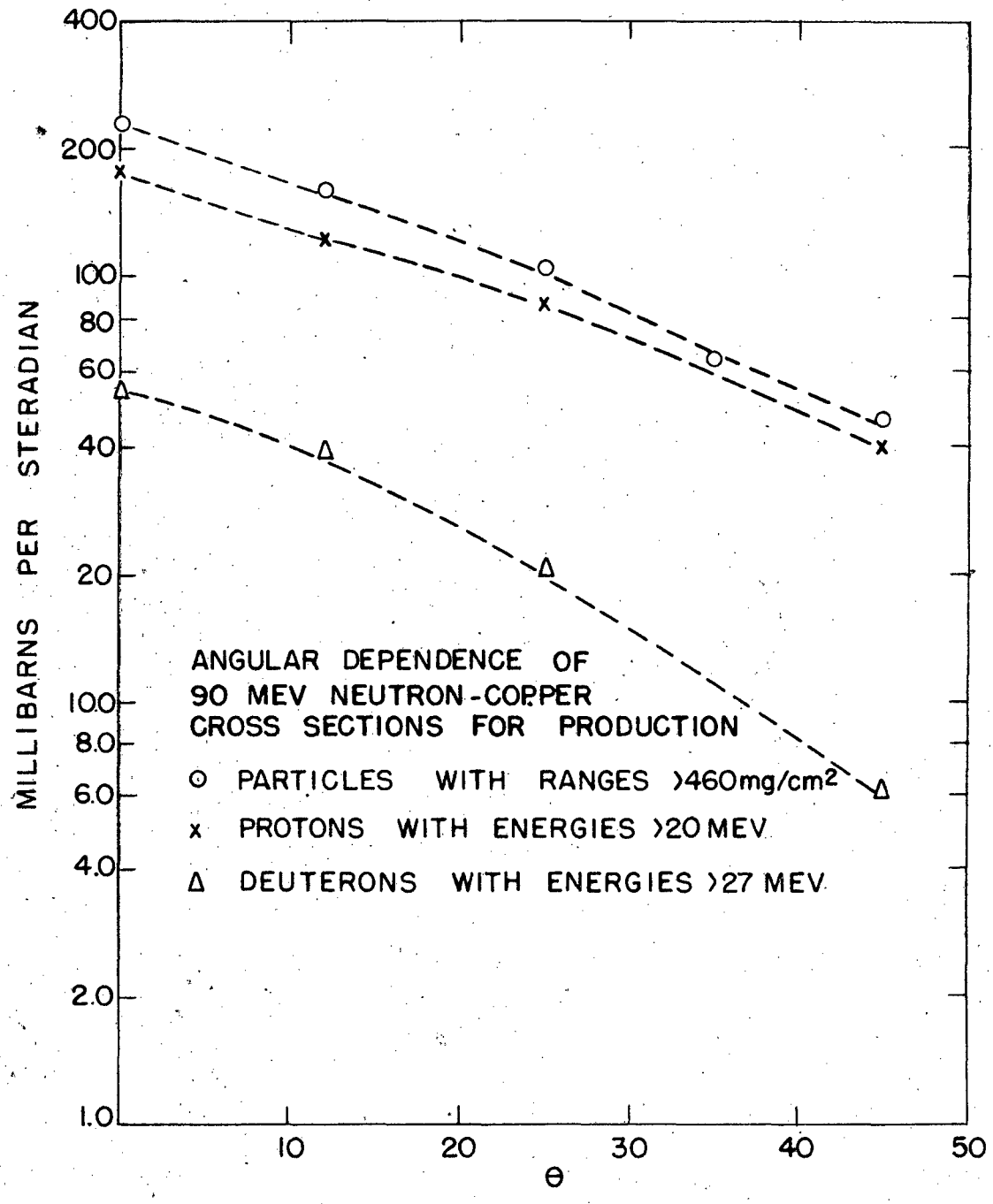
400
200
100
80
60
40
20
10.0
8.0
6.0
4.0
2.0
1.0
MILLIBARNS PER STERADIAN
ANGULAR DEPENDENCE OF
90 MEV NEUTRON-COPPER
CROSS SECTIONS FOR PRODUCTION
⊙ PARTICLES WITH RANGES >460mg/cm²
x PROTONS WITH ENERGIES >20 MEV
Δ DEUTERONS WITH ENERGIES >27 MEV
10
20
30
40
50
θ

FIG IX - 8

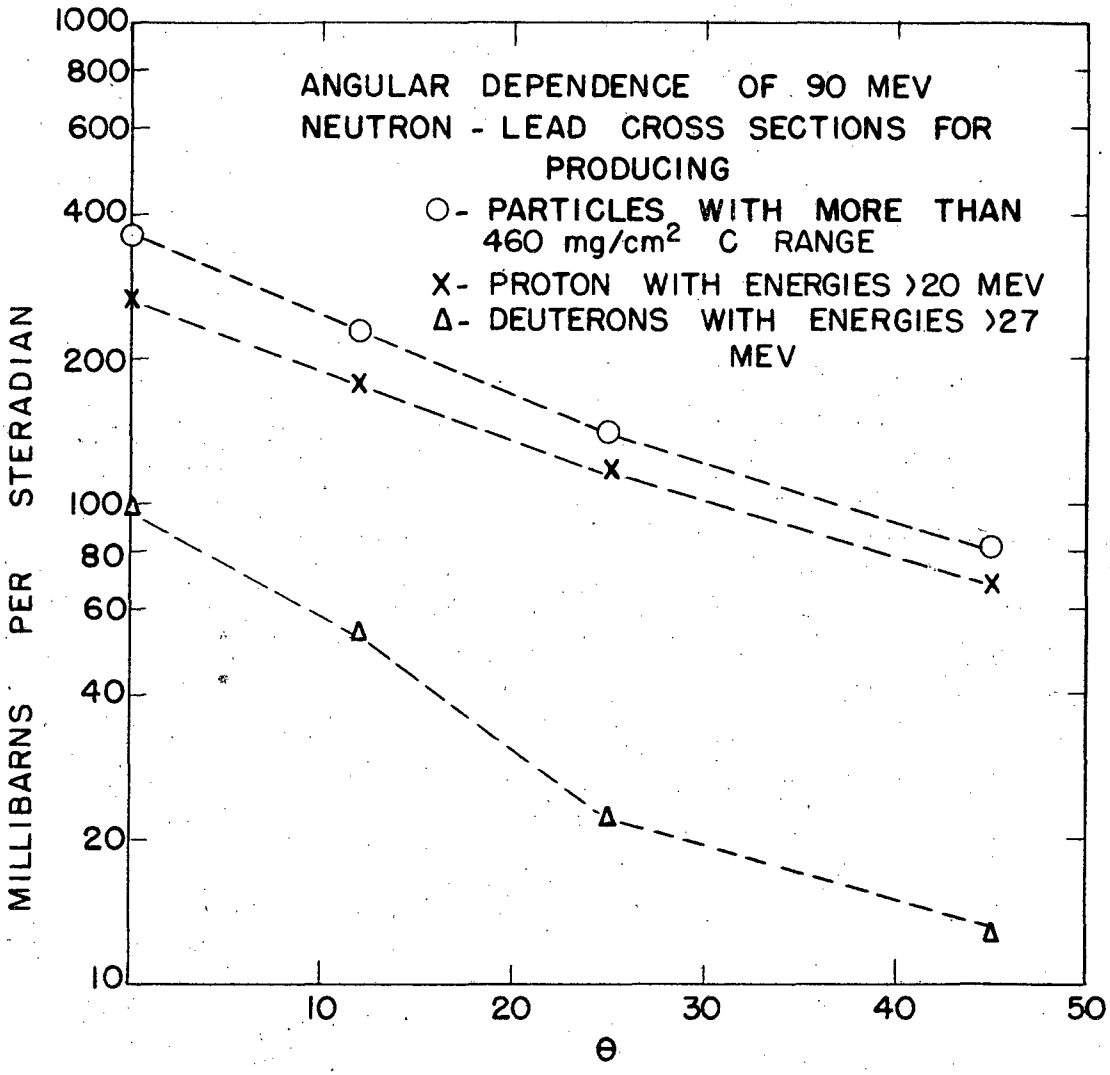
ANGULAR DEPENDENCE OF 90 MEV
NEUTRON - LEAD CROSS SECTIONS FOR
PRODUCING
○- PARTICLES WITH MORE THAN
460 mg/cm² C RANGE
X- PROTON WITH ENERGIES >20 MEV
Δ- DEUTERONS WITH ENERGIES >27
MEV
MILLIBARNS PER STERADIAN
1000
800
600
400
200
100
80
60
40
20
10
10
20
30
40
50
θ

FIG IX - 9

before, are seen to fall on a few straight line segments, and the ratio of protons to deuterons is seen to change smoothly with angle. It therefore seems reasonable to connect the values of $\frac{d\sigma_{x>E_a}(\theta)}{d\Omega}$ with straight lines, and to use the equations of these lines in integrating to find the total cross sections. In addition to the graphical arguments given above, the non-existance of singularities (except possibly at 0° where a singularity would not matter in these calculations) may also be deduced from the physics of the origin of these particles. The protons arise essentially from neutron proton collisions, and therefore must have an angular distribution of the type observed in n-p scattering, with an additional "smoothing out" effect due to the internal motion of the nucleons in the nucleus. Such a distribution would have no singularities, and, since the $\Sigma(\theta)$ curve is the sum of the proton and deuteron distributions, and since it shows no singularities between 6° and 135°, the deuteron distribution must also have no singularities in this range.

By integrating the appropriate parts of the curves in Figures IX-7 to IX-9, Table VII is derived. The table gives the total cross sections for producing the indicated particles within the indicated angular limits. The cross sections for producing deuterons between 45° and 180° (given in parentheses) are upper limits obtained by assuming the ratio between protons and deuterons found between 25° and 45° also holds from 45° to 180°. The corresponding proton cross section is then obtained by subtracting this deuteron cross section from the cross section for all particles, and is thus a lower limit.

TABLE VII
(All values are expressed in $10^{-27} cm^2$)

CARBON

	0°-25°	25°-45°	(0°-45°)	45°-180°	Total
All Particles	48	39	87	30	117
All Protons E 20 Mev	35	31	66	(24)	(90)
Protons E 35 Mev	24	19	43	(9)	(52)
All Deuterons E 27 Mev	12	8	20	(6)	(26)

COPPER

All Particles	88	82	170	123	293
Protons E 20 Mev	70	68	138	(103)	(241)
Deuterons E 27 Mev	18	14	32	(20)	(52)

LEAD

All Particles	123	153	276	223	499
Protons E 20 Mev	100	132	232	(192)	(424)
Deuterons E 27 Mev	23	21	44	(31)	(75)

X. DISCUSSION OF RESULTS

A. Shape of the Spectra

In the case of carbon, which is the only one for which there is such detailed information, the proton and deuteron spectra can be seen to be fundamentally different. The proton spectrum at zero degrees is flat from 20 Mev to about 65 Mev, and then it decreases sharply as the energy increases further. While it is obviously impossible to deduce from this curve (Figure IX-1), and the known neutron energy distribution, the spectrum which would be obtained for mono-energetic neutrons, it may be worthwhile to point out the rather striking similarity of the observed curve to that derived from a very simple assumption about the shape of the proton spectrum for such neutrons. This assumption is that for neutrons between 60 and 100 Mev, the proton spectrum in the forward direction is flat up to an energy equal to the neutron energy minus the energy required to make the reaction occur (about 15 Mev for 90 Mev incident neutrons) and then falls immediately to zero. On the basis of this assumption, the proton yield which would be obtained using neutrons with the energy distribution shown in Figure IV-1 would be essentially flat from 20 to 60 Mev, would fall to about one-half of the maximum value at 74 Mev, and to about one-eighth of this value at 90 Mev. All values of the observed spectra at 0° and 12° fit such a distribution within the probably errors shown.

The deuteron distribution at zero degrees shows a peak at about 60-65 Mev. The half-width of this peak in Mev is the same as the half-width of

of the neutron distribution, and the low energy tail is about twice as high relative to the peak as the low energy tail of the neutron beam. This distribution fits the assumption that mono-energetic neutrons produce deuterons within a relatively narrow energy range centered about 25 Mev below the neutron energy. As θ increases, the proton plateau and the deuteron peak both disappear. However, the average deuteron energy is higher than the average proton energy at all angles.

B. Total Cross Sections

The total cross sections for producing secondary protons with energy greater than 20 Mev as given in Table VII, are .090 barns for carbon, .24 barns for copper, and .42 barns for lead. The corresponding inelastic cross sections for 90 Mev neutrons as measured by DeJuren and Knable [3] are .22, .78, and 1.79 barns. The ratios of these cross sections are, therefore, .41 for carbon, .31 for copper and .24 for lead. Since the cross section for striking at least one proton in the nucleus must be proportional to the inelastic cross section, the decrease in this ratio must be due to the increased difficulty which a proton has in leaving the larger nuclei.

For the case of carbon only, an additional total cross section is given, namely, that for producing secondary protons with energies greater than 35 Mev. The reason for this particular choice of energy is the following: in the n-p scattering experiments performed at 90 Mev, the angular distribution of the scattered protons in the center of mass system is roughly

symmetric about 90^{0}. This symmetry means that in approximately one-half of the n-p collisions, the proton gets more than one-half of the energy the neutron had. Further, since the n-p collision cross section is supposed to be some three or four times larger than the n-n cross section, about .8 of the inelastic cross section should produce n-p collisions. Therefore, if the nucleus were completely transparent so that all struck protons could leave it without any further collisions, we should expect that about .4 of the inelastic cross section would produce protons with more than one-half of the energy available to protons. Then, since the maximum energy the proton can leave with is about 70 Mev (taking 85 Mev as the mean energy of the impinging neutrons), the cross section for producing secondary protons with energies greater than 35 Mev would be about .4 of the inelastic cross section if the nucleus were completely transparent to the struck protons. In the case of carbon this would be about 100 millibarns. The observed cross section for this process is 52 millibarns, and hence about one-half of the protons leave without further interaction. The above arguments are too qualitative to allow a calculation of the mean free path, but the result is in agreement with the mean free paths estimated by Fernbach[5] and Goldberger[6].

The total cross sections observed for deuteron production are given in Table VII as 26mb for C, 52 mb for Cu and 75 mb for Pb. The ratios of these deuteron production cross sections to inelastic cross sections are .12 for C, .067 for Cu and .042 for Pb, and hence the deuteron production

cross section also increases more slowly with atomic number than the inelastic cross section. They also increase more slowly than the cross sections for producing secondary protons, the ratio between the deuteron production cross sections and the proton production cross sections being .29, .22, and .18 for C, Cu, and Pb, respectively. This slower increase with Z is to be expected, since, in order for a deuteron to escape from a nucleus both of its component particles must escape without further interaction.

C. The Origin of the Secondary Protons

An attempt was made by M. L. Goldberger (6) to predict the energy and angular distributions of the protons which would be knocked out of heavy nuclei by 90 Mev neutrons. His calculations were made using the Monte Carlo method. The nucleus was treated as a degenerate gas of nucleons. The experimentally determined n-p differential cross sections were used to characterize the individual collisions which take place in the nucleus; the n-n interactions were assumed to lead to the same angular distribution as in n-p interactions, but with only one-fourth as large a total cross section. The angular distribution predicted by Goldberger gave a zero cross section for producing secondary particles straight forward (0°), and a maximum differential cross section at about 27°. The reason for the zero cross section forward was that small momentum transfers were forbidden by the Pauli principle, since the particle which received the small momentum would have to end up in a part of momentum space already occupied by

another particle. Such an angular distribution was not observed. A possible explanation, suggested by R. Serber, for the lack of a minimum in the forward direction is the following: the proton wave is refracted at the nuclear surface, since the proton passes from a region in which there is a high negative potential to a region in which there is zero potential. The effect of this refraction then completely washes out any detailed structure such as that predicted around zero degrees.

The energy distributions of the secondaries as predicted by Goldberger are also not confirmed by this experiment, the disagreement is presumably due to the fact that the correlation between angle and energy is again destroyed by the refraction effect.

The observed total cross section for producing secondary protons by bombardment of lead nuclei with 90 Mev neutrons is only about one-half of the predicted value. This indicates that the mean free path of particles in nuclear matter is smaller than the value given by Goldberger (6.2×10^{-13} cm) and is more nearly in agreement with that deduced by Fernbach et al [5] (4.5×10^{-13} cm).

D. The Origin of the Secondary Deuterons

A possible mechanism for the origin of the secondary deuterons has been suggested by G. F. Chew*. The principle feature of this mechanism is that the impinging neutron picks up a proton from the nucleus, and combines with it to form a deuteron. Semi-classically, the process may be described as follows: the protons in the nuclei have a large kinetic energy due to

*A similar suggestion has also been made by P. Gier et al[28].

their interactions with the other particles in the nucleus, and consequently may have large components of momenta in direction of the momentum of the impinging neutron. In fact, if the average kinetic energy of a bound nucleon is about 25 Mev, its average root mean square momentum will be about one-half $\left(\sqrt{\frac{25}{90}}\right)$ of the momentum of the impinging particle, and momenta equal to the neutrons momentum may easily be present. If, now, the difference between the momenta of the neutron and the proton is about equal the relative momentum of the proton and neutron in a deuteron, a deuteron may be formed. From the point of view above, the ideal situation would be that in which the relative momentum of the neutron and the proton was zero, since this is the most probable momentum in a deuteron. However, this situation is clearly impossible, since then the kinetic energy with which the deuteron left the nucleus would be twice that which the neutron brought in. Qualitatively, it can be seen that the energy of the deuteron would tend to be as high as energetically possible, and the angular distribution of the deuterons would be sharply peaked in the forward direction.

G. F. Chew, M. L. Goldberger, and G. Wick have made quantum-mechanical estimates of the cross section for the production of secondary deuterons, and have obtained values in qualitative agreement with the experimental results. Detailed comparisons between experiment and theory are complicated by several factors. Theoretical complications arise from the fact that this is essentially a many body problem since the residual nucleus must acquire some momentum as a whole in order to conserve this quantity, and

the potential energy of the resulting boron nucleus in the case of a $C^{12}(n,d)B^{11}$ reaction must be at least 15 Mev less negative than the potential energy of the carbon nucleus because of the highly endothermic nature of the reaction. Experimental complications arise from the fact that not only the original neutron can produce secondary deuterons, but the secondary protons and neutrons produced by the impinging neutrons can pick up a second particle and produce a deuteron on their way out of the nucleus. These deuterons would have in general a lower energy than those formed directly by the impinging neutron, and would have a much wider angular distribution. The yield of deuterons produced in this way could easily be as large or larger than the yield produced by the primary neutrons.

E. Comparison to Other Experiments

Experimental investigations of some of the phenomena reported in this paper have also been made by Brueckner and Powell [9] and Bradner[8]. Brueckner and Powell have made a could chamber study of the energy and angular distributions of the particles emitted by carbon nuclei under bombardment with 90 Mev neutrons. Their method involved the comparison of the $H\rho$'s of particle before and after passing thru a plate of known stopping power. They found high energy protons, deuterons and tritons, and their results are qualitatively in agreement with those obtained in the present experiment as regards the ratio of protons to deuterons and tritons, and the general trends of the energy and angular distributions.

There seems to be a quantitative disagreement in the absolute values of the various cross sections, however, the values found in the present experiment being considerably larger than those determined in the cloud chamber experiments.

Bradner's experiments were done using photographic plates, and were performed for the purpose of checking the existance of the secondary deuterons. The method involved a comparison of the grain density of tracks with the same residual range. The ratio of protons to deuterons in the forward direction as determined by his experiments is in agreement with that observed by Brueckner and Powell and in the present experiment.

F. Suggestions for Future Experiments

The various complications mentioned in Section D above would be completely removed in the case of n-D scattering experiments. A study of the deuterons scattered in the forward direction would thus provide an ideal way of studying the "pick up" process. Preliminary calculations by G. F. Chew indicate that the differential cross section for producing scattered deuterons by this process may be as high as 30 millibarns per steradian at zero degrees.

An experimental investigation of the secondary particles produced by neutrons with energies several times 90 Mev would also provide useful information. On the basis of the "pick up" theory, the deuteron yield should be much smaller than at 90 Mev. The proton distribution may be more nearly like that predicted by M. L. Goldberger since the mean free path will be

larger and refraction effects will be less important.

XI. ACKNOWLEDGMENTS

The author wishes to express his gratitude to Professor Segrè and the other members of the committee who guided this research for their frequent advice and encouragement. Thanks are also due to Professor E. O. Lawrence, Professor Serber, and Dr. B. J. Moyer for their continued interest in this work, to James Hadley, for his assistance in making the experimental observations and in setting up the experiments; to Clyde Wiegand, for the loan of certain equipment and for numerous suggestions; to Dr. Chew, Dr. Goldberger, and Dr. Serber for many interesting discussions of the theoretical implications of this work; and to the cyclotron crew, especially Mr. Vale and Mr. Watt, who kindly supplied some 10^{12} high energy neutrons.

REFERENCES

(1) N. Bohr, Nature 137, 344 (1936)

(2) Cook, L., E. McMillan, J. Peterson and D. Sewell, Phys. Rev., 72, 1264, (1947)

(3) DeJuren, J. and N. Knable. To be published in Phys. Rev.

(4) Bratenahl, A., R. Hildebrand, C. E. Leith and B. J. Moyer. To be published in Phys. Rev.

(5) Fernbach, S., R. Serber, and T. Taylor, Phys. Rev., 75, 1352, (1949)

(6) Goldberger, M. L., Phys. Rev., 74, 1269, (1948)

(7) This fact is based primarily on statistical considerations, i.e., n-p scattering can take place in both triplet and singlet states for all 's; p-p scattering only in singlet states for even 's. See for example reference 6.

(8) Bradner, H., Phys. Rev., 75, 1467, (1949)

(9) Brueckner, K., and W. Powell, Phys. Rev., 75, 1274, (1949)

(10) York, H., Phys. Rev., 75, 1467, (1949)

(11) Morand, M., P. Cüer, and H. Moucharafyeh, Comptes rendus, 226, 1008, 1948 and Powell, C. F., and L. Leprince-Ringuet, Cosmic Ray Conference, Bristol, (1948)

(12) Serber, R., Phys. Rev., 72, 1007 (1947)

(13) Dexter, E., and M. Sands, LADC 414, (Los Alamos)

(14) Hadley, J., E. Kelly, C. Leith, E. Segre, C. Wiegand and H. York., Phys. Rev., 75, 351, (1949)

(15) Brueckner, K., W. Hartsough, E. Hayward, and W. Powell, Phys. Rev., 75, 555, (1949)

(16) Diven, B. C., and B. Rossi, LADC 148, Los Alamos, (1944)

(17) Aron, W., B. Hoffman and F. Williams, UCRL 121 Revised, Nov. 1948

(18) Cüer, P., M. Morand, and L. Van Rossum, Comptes rendus, 228, 481, (1949)